Principles and applications of ENDOR spectroscopy for structure determination in solution and disordered matrices

Damien M. Murphy* and Robert D. Farley†

Received 2nd August 2005
First published as an Advance Article on the web 24th January 2006
DOI: 10.1039/b500509b

Both electron paramagnetic resonance (EPR) and electron nuclear double resonance (ENDOR) spectroscopies are extremely powerful and versatile methods for the characterisation of paramagnetic systems in biology, chemistry, and physics. However, by comparison to EPR, ENDOR remains a less widely used technique. In this *tutorial review* the basic principles of continuous wave ENDOR are described. The theory of orientation selective ENDOR, for structure determination in frozen solutions and powders, is then described. A range of examples, illustrating the type of information obtained from the ENDOR spectrum, is finally presented.

1 Introduction

The electron spin of a transition metal ion can interact with ligand nuclear spins *via* dipolar and Fermi contact interactions, producing shifts in the NMR lines of the ligand nuclei. The dipolar interaction depends on the relative position of the nuclear spins with respect to the metal atom, so the NMR spectrum can yield information on nuclear co-ordinates. However, this is not always easy for a paramagnetic complex, because the presence of the unpaired electron will broaden the NMR lines considerably. In that case, EPR or ENDOR spectroscopy is required to study the system.

School of Chemistry, Cardiff University, Main Building, Park Place, Cardiff, UK CF10 3AT
† Current address: Radiotherapy Physics Department, University Hospital of North Staffordshire, NHS Trust

Electron **P**aramagnetic **R**esonance (**EPR**) spectroscopy is used to study systems containing unpaired electrons,[1] but one major drawback of EPR, however, is the low resolution which results from line broadening and line splitting effects due, in part, to the couplings of the electron spins to many surrounding nuclear spins. These electron-nuclear couplings are however an important parameter in the investigation of paramagnetic systems, in order to obtain information on the ligand co-ordinates. As stated above, this information cannot be obtained through the NMR technique primarily because of the greatly increased linewidths caused by the presence of the unpaired electron. This problem can be eliminated by performing a double resonance experiment, by detecting the NMR resonances *via* intensity changes of a simultaneously irradiated EPR line. In this **E**lectron **N**uclear **DO**uble **R**esonance (ENDOR) experiment, the NMR quanta are detected in the microwave, rather than the RF range (known

Damien M. Murphy

Damien M. Murphy obtained a Diploma in Applied Science (Chemistry) in 1989 and later GRSC (II) Degree in 1990 from the Dublin Institute of Technology, Ireland. He studied for his PhD at the University of Turin, Italy under the guidance of Prof. E. Giamello from 1990–1993. After postdoctorate periods at the Instituto Superior Técnico, in Lisbon, Portugal (1994), and the Université P. et M. Curie, in Paris, France (1995) he moved to Cardiff University as a Lecturer in Physical Chemistry in 1996 and later senior lecturer in 2002. He was secretary of the ESR group of the RSC from 1998–2003, and Manager of the National ENDOR service from 1996–2003. His current research interests are the characterisation of heterogeneous and homogeneous catalysts by EPR and ENDOR spectroscopy.

Robert D. Farley

Robert D. Farley obtained his BSc. in Chemistry at the University of York in 1990 and later remained at York to study for his DPhil (awarded 1994) under Prof. B. C. Gilbert and Dr P. Hanson; he then moved to the Physikalisch-chemisches Institut der Unversität Zürich as a postdoctoral fellow. In 1996 he took up the post of Research Associate at the National ENDOR Service at Cardiff University where he developed an interest in the use of ENDOR spectroscopy for the determination of molecular structure. In 2003 he moved to Staffordshire, retrained and now works in the Radiotherapy Physics Department at the University Hospital of North Staffordshire NHS Trust. His current research interests are concerned with conformity and organ motion in intensity modulated radiotherapy.

as quantum transformation) resulting in a sensitivity enhancement of several orders of magnitude over conventional NMR spectroscopy. Therefore, ENDOR can be regarded as NMR spectroscopy on an EPR spectrometer.

ENDOR offers many advantages, compared to EPR, for the structural characterisation of paramagnetic systems in solution and in the solid state. One very important advantage of the technique is the resolution enhancement gained for organic radicals in solution. In general, each group of equivalent nuclei (regardless of how many nuclei belong to this group) contributes only two lines to the ENDOR spectrum. Addition of nonequivalent nuclei to the paramagnetic system causes a multiplicative increase in the number of lines in the EPR spectrum, but only an additive increase in the ENDOR spectrum. For example, the solution EPR spectrum of the radical cation of 9,10-dimethylanthracene theoretically produces 175 lines due to the three sets of inequivalent protons (Fig. 1). Simulation of the spectrum is required in order to extract the hyperfine couplings constants, but this is often far from trivial. By comparison, the ENDOR spectrum produces only three pairs of lines (one for each set of equivalent nuclei) from which the hyperfine couplings can be determined directly. As seen from this simple example, the ENDOR spectrum simplifies considerably the analysis of complex EPR spectra. Furthermore, since each ENDOR resonance is centred about the field dependent nuclear Larmor frequency of the nucleus, exact identification of the interacting nucleus can be obtained.

Another major advantage of the ENDOR technique, is the ability to obtain structural information from the powder EPR spectra of metal complexes or paramagnetic proteins in frozen solution. The most sensitive probe for structure determination is the electron nuclear hyperfine interaction tensor, and this can be obtained using ENDOR spectroscopy. The frozen solution EPR spectrum (or powder spectrum) is composed of a superimposition of the individual resonances from the randomly oriented molecules in which the applied magnetic field assumes all possible orientations with respect to the molecular frame. When an ENDOR measurement is made at a selected field position in the EPR spectrum it comprises only that subset of molecules having orientations that contribute to the EPR intensity at the chosen value of the observing field. If EPR turning points are selected, namely magnetic field values which correspond to defined molecular orientations, so called ''single crystal like'' ENDOR spectra can be obtained. In this ''angular selective'' or ''orientation selective'' ENDOR experiment, the principal components of the magnetic tensors for each interacting nucleus can be obtained by simulation of the data, and this information can be used to provide structural information on the distance and spatial orientation of the remote nucleus. This ability to obtain three dimensional structure is extremely important for paramagnetic systems lacking long range order or in cases where single crystals cannot be prepared.

The purpose of this tutorial review will be (i) to present the basic principles of cw-ENDOR spectroscopy for radicals in solution, (ii) to describe the basic theory of orientation selective ENDOR for paramagnetic species in frozen solution, and (iii) to provide some illustrative examples. A number of excellent textbooks[2–5] and reviews[6–8] are available which provide a detailed description of the theory of ENDOR. The theory of orientation selective ENDOR spectroscopy has been discussed in several articles,[9–11] while the applications of this methodology for structure determination in paramagnetic proteins and biomolecules has recently been reviewed.[12–15] It should be noted here that ENDOR measurements can be conducted both in the continuous wave (cw-) or time domain

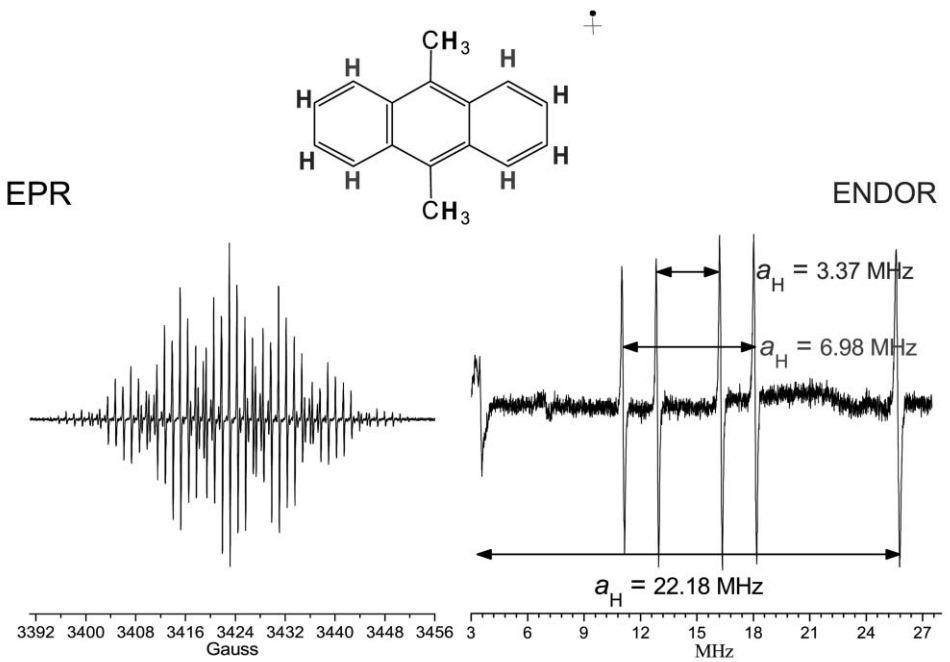

Fig. 1 cw-EPR spectrum and corresponding ^{1}H ENDOR spectrum of the radical cation of 9,10-dimethylanthracene in fluid solution.

(pulsed-) mode. This review will only treat cw-ENDOR, and the interested reader is referred to a number of excellent reviews and recent textbook on the subject of pulsed electron paramagnetic resonance.[16–18]

2 Basic principles of cw-ENDOR

In a simple EPR experiment, one observing frequency (microwave) is used to excite the EPR transition. In a multiple resonance experiment two or more irradiating fields are used to excite different transitions simultaneously. The oldest and most widely used multiple resonance technique is ENDOR, which was introduced for solids by Feher in 1956[19] and later by Hyde and Maki[20] for liquids. In ENDOR, one monitors the effects on an EPR transition of a simultaneously driven NMR transition and thus one essentially detects the NMR absorption with much greater inherent sensitivity than EPR. In order to explain how the technique works, one must consider the appropriate energies for the simplest case of a two spin system (*i.e.*, one electron and one proton) interacting with an applied magnetic field. The simplified spin Hamiltonian for this two spin system ($S = ½$, $I = ½$) in an external applied field $\boldsymbol{B}_0$ is given as:

$$H = H_{EZ} + H_{NZ} + H_{HFS} \tag{1}$$

where EZ = electron Zeeman term, NZ = nuclear Zeeman term, and HFS = hyperfine interaction. This equation takes the form;

$$H = \mu_B \boldsymbol{B}_0 \cdot \boldsymbol{g} \cdot \boldsymbol{S} - g_n \mu_n \boldsymbol{B}_0 \cdot \boldsymbol{I} + h \boldsymbol{S} \cdot \boldsymbol{A} \cdot \boldsymbol{I} \tag{2}$$

where g_n is the nuclear g-factor, $\boldsymbol{S}$ and $\boldsymbol{I}$ are the vector operators of the electron and nuclear spins, μ_B (commonly written as β_e in the literature) is the Bohr magneton (9.274×10^{-24} J T^{-1}), μ_n is the nuclear magneton (5.05×10^{-27} J T^{-1}), h is the Planck constant (6.626×10^{-34} J s) and $\boldsymbol{g}$ and $\boldsymbol{A}$ are the g- and hyperfine coupling tensors. Assuming only isotropic interactions and with the external magnetic field aligned along the Z axis, the following expression is obtained:

$$H = g\mu_B B_0 S_Z - g_n \mu_n B_0 I_Z + ha \boldsymbol{S} \cdot \boldsymbol{I} \tag{3}$$

where g is the dimensionless isotropic g-factor and a is the isotropic hyperfine coupling constant in hertz (Hz), not to be confused with $A/g\mu_B$ which is the hyperfine splitting in field units. Ignoring second order terms, and in the high field approximation, the energy levels for the two spin system ($S = ½$, $I = ½$) can be defined as:

$$E\,(M_S, M_I) = g\mu_B B_0 M_S - g_n \mu_n B_0 M_I + ha M_S M_I \tag{4}$$

where M_S and M_I are the magnetic spin quantum numbers, with values of $\pm ½$. For simplicity, the electron and nuclear Zeeman energy terms can be expressed in frequency units giving:

$$E(M_S,M_I)/h = \nu_e M_S - \nu_n M_I + a M_S M_I \tag{5}$$

where $\nu_e = g\mu_B B_0/h$ and $\nu_n = g_n \mu_n B_0/h$. The four possible energy levels resulting from this equation (labelled $E_a - E_d$) can be written as follows:

$$E_a = - ½ g\mu_B B_0 - ½ g_n \mu_n B_0 - ¼ ha \tag{6a}$$

$$E_b = + ½ g\mu_B B_0 - ½ g_n \mu_n B_0 + ¼ ha \tag{6b}$$

$$E_c = + ½ g\mu_B B_0 + ½ g_n \mu_n B_0 - ¼ ha \tag{6c}$$

$$E_d = - ½ g\mu_B B_0 + ½ g_n \mu_n B_0 - ¼ ha \tag{6d}$$

By application of the EPR selection rules ($\Delta M_I = 0$ and $\Delta M_S = \pm 1$), it is found that two possible resonance transitions can occur, namely ΔE_{cd} (labelled EPR 1) and ΔE_{ab} (labelled EPR 2), as shown in Fig. 2:

$$\Delta E_{cd} = E_c - E_d = g\mu_B B - ½ ha \tag{7a}$$

$$\Delta E_{ab} = E_b - E_a = g\mu_B B + ½ ha \tag{7b}$$

These two transitions give rise to two absorption peaks at different magnetic field positions and are separated by a, the isotropic hyperfine splitting. The energy levels in Fig. 2 are labelled by the sign of the simple product function $|M_S, M_I>$ (*e.g.*, $|+ ->$ denotes $M_S = +½$ and $M_I = -½$). We now see that the two allowed EPR transitions are again $E_c \leftrightarrow E_d$ and $E_b \leftrightarrow E_a$, *i.e.*,

$$\nu_{EPR} = \nu_e \pm a/2 \tag{8}$$

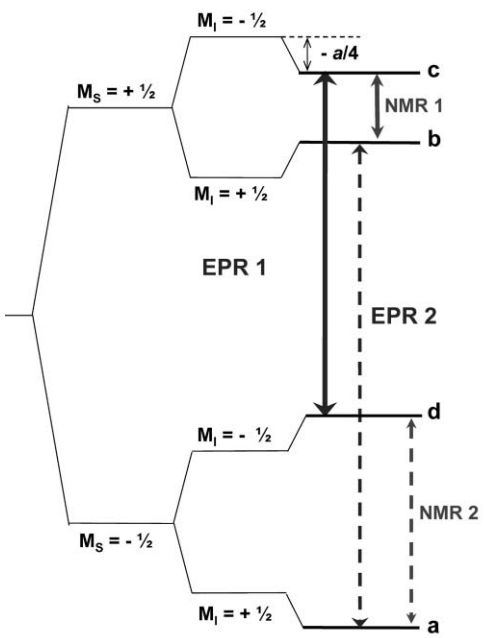

Fig. 2 Energy level diagram for a two spin system ($S = ½$ and $I = ½$) in high magnetic field, illustrating the electron Zeeman, nuclear Zeeman and hyperfine splittings. a is the isotropic hyperfine coupling (where $a > 0$ and $|a/2| < \nu_n$). The two EPR transitions (labelled 1 and 2) obey the selection rules $\Delta M_S = \pm 1$, $\Delta M_I = 0$, while the two NMR transition (1 and 2) obey the selectrion rules $\Delta M_I = \pm 1$, $\Delta M_S = 0$.

Table 1 Nuclear spin quantum numbers and nuclear Larmor frequencies at X-band (9 GHz) and Q-band (35 GHz) for a range of commonly studied nuclei

Nucleus	Abundance (%)	Spin (I)	ν_n/MHz for 3.5 kG field	ν_n/MHz for 12.5 kG field
^{1}H	99.985	½	14.90218	53.22207
^{2}H	0.0148	1	5.585691	19.94889
^{11}B	80.2	⅔	4.782043	17.07872
^{13}C	1.11	½	3.74795	13.38553
^{14}N	99.63	1	1.077201	3.847146
^{15}N	0.366	½	1.511052	5.396614
^{17}O	0.038	⅖	2.02099	7.21782
^{19}F	100	½	14.02721	50.09717
^{31}P	100	½	6.03804	21.56442

If we now consider the NMR transitions, we can apply the NMR selection rules $\Delta M_I = \pm 1$ and $\Delta M_S = 0$, yielding two NMR transitions (labelled NMR 1 and 2 in Fig. 2) at the frequencies:

$$\nu_{NMR} = |\nu_n \pm a/2| \quad (9)$$

It is these NMR transitions that are detected by ENDOR *via* the intensity changes to the simultaneously irradiated EPR transition. It is important to note, that both the hyperfine coupling constant (a) and the nuclear Larmor frequencies (ν_n) are determined in the ENDOR experiment. Therefore, unlike the situation in EPR, the hyperfine couplings can be measured with higher resolution and accuracy, and can also be directly assigned to a specific nucleus since the values of ν_n are specific to individual nuclei (see Table 1). For many nuclei, ν_n values occur at low frequencies (less than 5 MHz) so the assignments are often complicated in multi-nuclear systems due to overlapping signals from different nuclei. Since ν_n is field dependent, it is often beneficial to perform the ENDOR measurementrs at higher frequencies (*e.g.*, 35 GHz and 90 GHz).

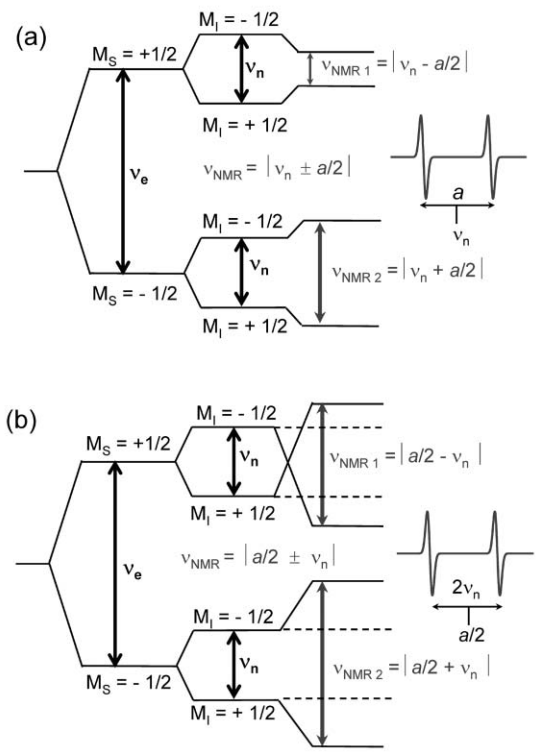

Fig. 3 Energy level diagram for a two spin system (S = ½ and I = ½) in high magnetic field illustrating the electron Zeeman, nuclear Zeeman and hyperfine splitting for the two cases where (a) $a > 0$ and $a/2 < \nu_n$, and (b) $a > 0$ and $a/2 > \nu_n$. The frequency of the two resulting ENDOR lines are given by $\nu_{NMR} = |\nu_n \pm a/2|$ in (a) and $\nu_{NMR} = |a/2 \pm \nu_n|$ in (b).

In the above example (S = ½, I = ½), two ENDOR lines are detected, equally spaced about ν_n and separated by the hyperfine coupling constant. This pattern occurs in the case where $\nu_n > |a/2|$. In the case where $\nu_n < |a/2|$, the energy level diagram must be changed and then two ENDOR lines are observed, centred around $a/2$ and separated by $2\nu_n$ (Fig. 3).

In the above example, two lines were observed both in EPR and in ENDOR. To illustrate resolution enhancement of ENDOR, more complex energy level diagrams are required. A good example is the *para*-benzoquinone radical anion (Fig. 4). In this radical, the four equivalent protons produce a quintet of lines in the EPR spectrum, but only two lines are observed in the ENDOR spectrum, since all NMR transitions in the same M_S manifold are degenerate.

Each group of equivalent nuclei therefore contributes only two ENDOR lines to the spectrum. Addition of non-equivalent nuclei to the system has a multiplicative increase in the number of signals in the EPR spectrum (eqn (10)), but only an additive increase in the ENDOR (eqn (11)). This enhancement in spectral resolution can be expressed quantitatively as:

$$\text{Spectral density}_{EPR} = \frac{\prod_{i=1}^{k}(2N_iI_i+1)}{\sum_{i=1}^{k}2|a_i|N_iI_i} \quad (10)$$

$$\text{Spectral density}_{ENDOR} = \frac{2k}{|a_{max}|} \quad (11)$$

where there are k groups of i equivalent nuclei of nuclear spin I_i and a number of nuclei N_i in each group; a_{max} denotes the largest hyperfine coupling constant, which in a homonuclear ENDOR experiment is equal to the spectral width. Therefore, resolution enhancement is offered by the ENDOR experiment only when non-equivalent nuclei are present. It should be noted, that while EPR suffers from low resolution for large numbers of interacting nuclei, ENDOR provides high resolution but lower sensitivity compared to EPR. This can be seen by comparison of the EPR and corresponding ENDOR spectra for the phenalenyl radical in solution (Fig. 5). The radical has two sets of inequivalent protons (*i.e.*, a set of 6 and a set of 3 protons). Since the number of lines produced in an EPR spectrum is $2nI + 1$, where n = number of equivalent nuclei, the first set of protons produces a septet of lines and the second set of protons produces a quartet of lines. The EPR spectrum is thus composed of $7 \times 4 = 28$ lines. The ENDOR measurement is then performed by locking the magnetic field onto one of the EPR lines (usually the most intense line), increasing the microwave (MW) absorption until the EPR

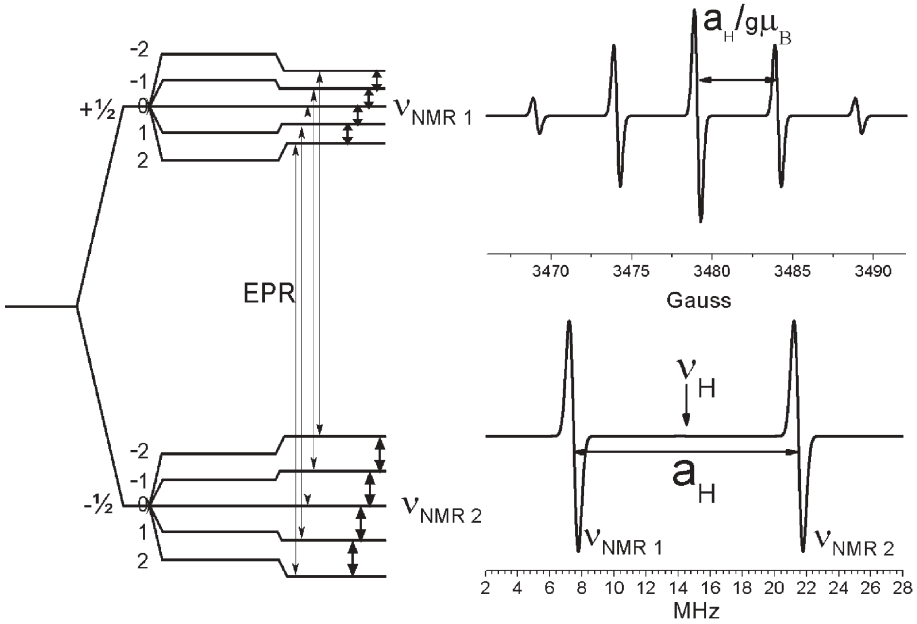

Fig. 4 Energy level diagram for an $S = ½$ spin system interacting with four equivalent $I = ½$ nuclei showing the solution EPR and corresponding ENDOR spectra (where $a > 0$ and $|a/2| < \nu_n$). Note; the isotropic hyperfine splitting ($a_H/g\mu_B$) is given in field units (Gauss) in the EPR spectrum whereas the isotropic hyperfine coupling constant (a_H) is given in frequency units (MHz) in the ENDOR spectrum.

signal just begins to saturate and sweeping the radiofrequency (RF). The resulting ENDOR spectrum produces only four lines, with separations of 5.09 MHz and 17.67 MHz (both centred on ν_n) and therefore a significantly simplified analysis.

It can be seen from the above example, that by applying more than one selection rule to the spin system, a significant improvement in spectral resolution is achieved by "elimination of redundancy". However, it is worth noting at this point that

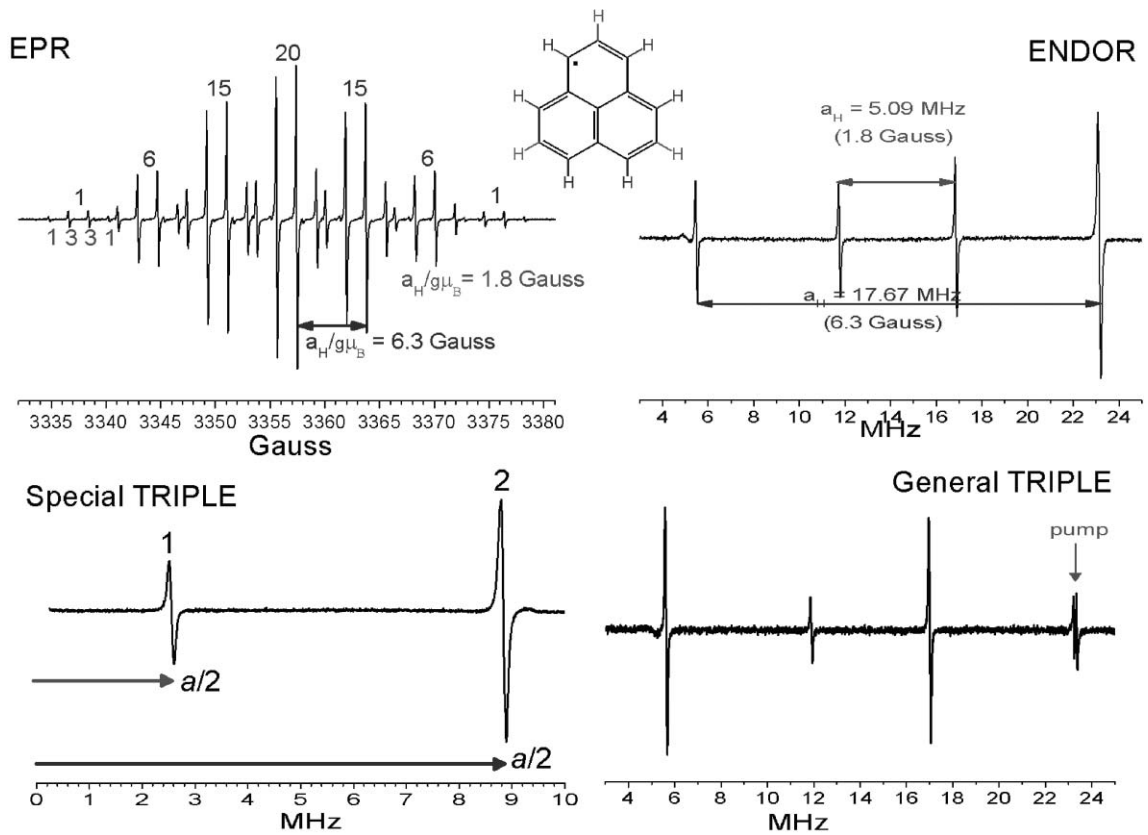

Fig. 5 EPR, ENDOR, special TRIPLE and general TRIPLE resonance spectra of the phenalenyl radical recorded at room temperature in mineral oil.

the ENDOR spectrum does not contain any information about the number of nuclei contributing to a given transition. This can be retrieved by multi-electron nuclear resonance techniques (section 2.3).

2.1 Level population and a simple description of the ENDOR effect

In an ENDOR experiment, the NMR transitions are not observed directly but rather indirectly *via* the changes to the microwave absorption of a simultaneously irradiated EPR transition, as described above. To illustrate this effect more clearly, one must consider the population difference between the four energy levels in our simplified two spin system ($S = ½$, $I = ½$). The relative populations of the four hyperfine levels (a, b, c and d) in Fig. 2, at thermal equilibrium are given by the Boltzmann law. At temperatures above a few kelvin, the electronic Boltzmann factor can be described as;

$$N_b/N_a = \exp(-g\mu_B B_0/kT) = 1 - g\mu_B B_0/kT \qquad (12)$$

The difference between the nuclear spin levels (c,b and d,a) can be neglected since these differences are of the order of $g_n\mu_n B_0/kT$, which is only about 10^{-3} of the population difference between the electronic levels (c,d and b,a). If ε is defined as $g\mu_B B_0/kT$, the initial population difference between the upper and lower levels is shown in Fig. 6a (*i.e.*, a slight excess in the lower level represented as $1 + \varepsilon$, and a slight depletion in the upper level represented as $1 - \varepsilon$).

The thermal populations in levels a and b will remain the same provided the EPR transition a $\rightarrow$ b is induced with sufficiently low microwave power (Fig. 6a). In this case, the induced transition rate a $\rightarrow$ b cannot compete with the efficient spin–lattice relaxation, causing the ''hot spins'' to return from b $\rightarrow$ a. As the microwave power is increased (schematically represented by the thicker line labelled EPR 2 in Fig. 6b), the induced absorption rate can now compete with the electronic spin relaxation rate, and saturation of the levels a and b occurs with the resulting equalization of the relative populations (Fig. 6b). In reality complete saturation is seldom achieved, as

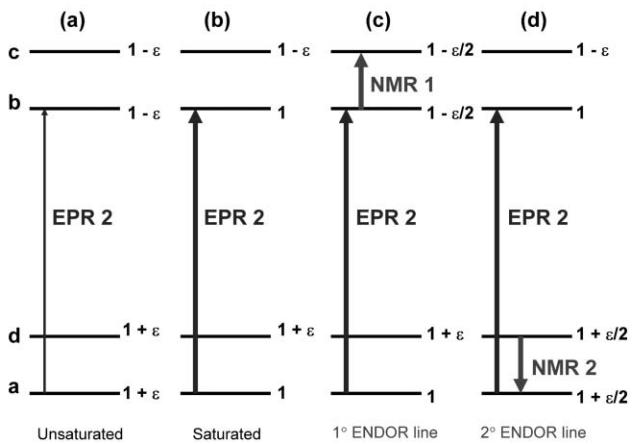

Fig. 6 Four level energy diagram for a two spin system ($S = ½$ and $I = ½$). The four levels a, b, c and d correspond to the same energy levels as represented in Fig. 2.

the EPR signal would completely disappear, but at least a much smaller EPR signal is observed under these partially saturated conditions. If a nuclear radiofrequency is now applied between levels b and c, the EPR line becomes desaturated (*i.e.*, restoration of the population difference between a and b) *via* induced absorption, which equalizes the populations of levels b and c (Fig. 6c). The net result is an increase in the inequality in the populations of the two energy levels corresponding to the EPR transition, namely levels a and b. In other words, the application of the nuclear radiofrequency, partially desaturates the EPR signal, and thereby increases the EPR response. This increase in the EPR signal constitutes an ENDOR response, and the first ENDOR line is observed corresponding to the NMR 1 frequency. If the nuclear radiofrequency is subsequently applied between levels a and d, the EPR signal is also desaturated, by induced emission, and a second ENDOR signal appears, corresponding to the NMR 2 frequency. The partial desaturation of the EPR signal by the RF field can be regarded as a decrease in the effective spin lattice relaxation time. This decrease is characteristic of the most general type of ENDOR mechanism.

As stated above, in the ENDOR experiment, the nuclear resonances are not observed directly but rather indirectly *via* their influence on the EPR line (known as a quantum transformation). In other words, a quantum transformation occurs from the low frequency domain (where spin transitions occur) to the high frequency domain, where the absorbed energy is detected. This detection scheme leads to an intensity enhancement of the signals that is $\sim 10^3$ times higher that the NMR experiment. In this simple description of ENDOR, relaxation effects are neglected, but in reality, in the presence of a saturating MW and RF field all three energy levels a, b and c would become equally populated after a short time and the ENDOR signal would disappear (*i.e.*, producing a *transient* ENDOR response). In order to observe a continuous ENDOR response, a complete relaxation pathway for the electron spins, that parallels the spin lattice pathway, must be available. One such mechanism for relaxation is shown as the *steady state* ENDOR effect.

2.2) The steady state ENDOR effect

In order to consider the steady state mechanism of ENDOR, one must first consider the various relaxation pathways available for the simple two spin system described earlier (Sv$= ½$, $I = ½$). These relaxation pathways are illustrated in Fig. 7. The solid lines represent radiation induced transitions, while the dashed lines represent radiationless electron spin–lattice (W_e), nuclear spin–lattice (W_n) and cross relaxation processes ($W_{\times 1}$ and $W_{\times 2}$). W_e and W_n are the inverse of the spin lattice relaxation $W_i = 1/T_1$. $W_{\times 1}$ and $W_{\times 2}$ represent cross relaxation effects when both electron and nuclear transitions occur simultaneously, *i.e.*,

$$W_{\times 1} = |+ -> \rightarrow |- +> \text{ (}i.e.\text{, 'flip flop' transition)} \qquad (13a)$$

$$W_{\times 2} = |+ +> \rightarrow |- -> \text{ (}i.e.\text{, 'flop flop'transition)} \qquad (13b)$$

In ENDOR, the EPR transition ($\nu_{EPR\ 1}$) is irradiated with MW power high enough to ensure that the spin lattice radiation rate W_{eI} does not compete with the induced transition. The signal is

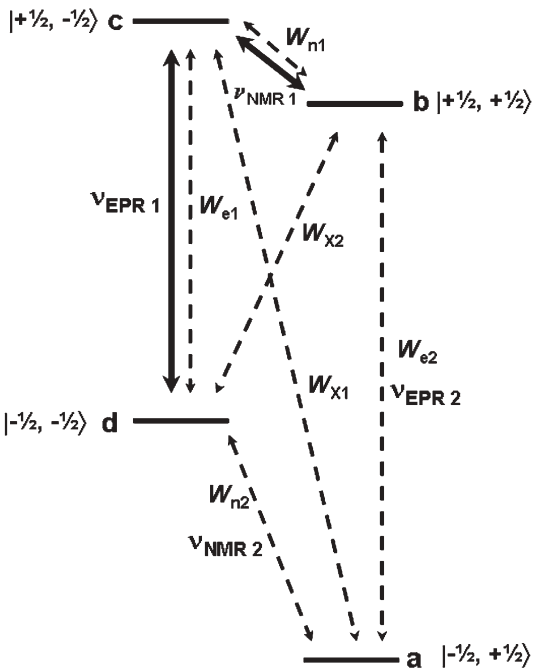

Fig. 7 Four level energy diagram for a two spin system (S = ½ and I = ½). The four levels a, b, c and d correspond to the same energy levels as represented in Fig. 2. Solid lines = induced transitions; dotted lines = relaxation transitions.

partially saturated as the Boltzmann populations equalize. The most effective route for electron relaxation from c → d is pathway W_{e1}. However, another possible route is c → b → a → d known as the *bypass route*. This route is not effective in normal EPR experiments, as the nuclear relaxation rate W_{n1} and W_{n2} are much less that W_{e1} (causing a build up of spins in levels b and d). The '*bottleneck*' caused by W_{n1} may be partially removed by pumping the transition c → b with a saturating RF field (of frequency $\nu_{NMR\ 1}$), which effectively short circuits W_{n1}. This improves the efficiency of the bypass route, increases the effective spin lattice relaxation rate, and so leads to desaturation of the EPR transition and a corresponding increase of the EPR signal intensity. It is exactly this effect that is detected in the ENDOR experiment. This is known as the *steady state ENDOR effect*.

The magnitude (or enhancement) of the EPR response clearly depends on the relative rates W_e, W_n, $W_{\times 1}$ and $W_{\times 2}$. Neglecting $W_{\times i}$ (eqns (13a) and (13b)) optimum ENDOR signals are observed when $W_e = W_n$ as no relaxation bottleneck appears in the bypass route. The rates W_e and W_n depend differently on the rotational correlation (τ_R) for Brownian diffusion since $W_e \propto 1/\tau_R$ and $W_n \propto \tau_R$. As a result the two relaxation rates can be fine-tuned by altering the temperature and viscosity of the solvent. This can be understood with respect to the Debye–Einstein equation, which relates τ_R to the effective molar volume ($V_{eff} = 4/3\pi r^3$), the viscosity of the solvent and the temperature where $\tau_R = V_{eff}(\eta/k_BT)$. As the temperature decreases, and η increases, then W_e becomes smaller and W_n larger. The optimum ratio corresponds to the situation where $W_n/W_e \cong 1$. For protons, $W_n <<< W_e$, so optimum ENDOR occurs in solvents of low viscosity (such as toluene, THF, *etc.*) near the freezing points. For solvents of high viscosity, ENDOR signals can be observed at ambient temperatures.

2.3 Brief overview of multiple electron nuclear resonance techniques

ENDOR is a double resonance experiment, because two transitions (an EPR and an NMR) are excited simultaneously. However, conceptually it is possible to extend the number of transitions excited simultaneously and so perform a multiple resonance experiment, where more than two transitions are simultaneously excited. One such multiple resonance experiment is called electron–nuclear–nuclear triple resonance, generally abbreviated to TRIPLE resonance. There are two types of TRIPLE experiment that can be performed; *special* TRIPLE, in which both ENDOR transitions associated with a particular hyperfine interaction are simultaneously excited, and *general* TRIPLE, in which one particular ENDOR transition is pumped with one RF field while all the other ENDOR transitions are monitored with a second RF field. The information gained by performing these TRIPLE experiments, ranges from a significant enhancement in sensitivity of the signals to determining the signs of the hyperfine couplings.

2.3.1 Special TRIPLE resonance. The mechanism of the ENDOR response was explained above (section 2.2) as arising from a short circuiting of one of the two relaxation bottlenecks in the bypass route c → b → a → d (*i.e.*, either transition ν_{NMR1} or ν_{NMR2} in Fig. 7). However, a substantial enhancement in the EPR signal intensity should be achieved if *both* NMR relaxation bottlenecks are *simultaneously* pumped with an RF field. Since the optimum ENDOR response is obtained when $W_n = W_e$, this short-circuiting of the two NMR transitions leads to a substantial enhancement in sensitivity (up to 100% of the EPR intensity under favourable conditions). Resolution enhancement is also possible in the resulting special TRIPLE spectrum since the effective NMR saturation is smaller in TRIPLE compared to ENDOR for a given power level, so narrower lines can be observed compared to ENDOR (the lineshape of a TRIPLE spectrum being essentially Lorentzian squared). Another very important advantage of special TRIPLE is that the signal intensities can reflect the ratio of the numbers of equivalent nuclei (when $W_{n(driven)} \gg W_e \gg W_n$).

The actual experiment is performed by irradiating the sample simultaneously with two RF fields in the presence of the saturating MW radiation. Starting at the nuclear Larmor frequency of interest, one RF field is swept to high frequency while the second is simultaneously swept to lower frequencies. As a result both NMR transitions for each set of equivalent nuclei are excited at the same time. Therefore a single special TRIPLE resonance peak is observed (instead of two peaks in ENDOR), separated from the origin of the NMR frequency axis ($\nu_{NMR} = 0$) by the frequency $|a/2|$ with different intensities which reflect the number of nuclei in each inequivalent set. An example of a special TRIPLE resonance spectrum for the

phenalenyl radical is shown in Fig. 5. The peaks are observed at 2.545 MHz and 8.835 MHz (*i.e.*, $a/2$ for both hyperfine couplings) with a relative intensity ratio of 1 : 2 reflecting the 3 : 6 ratio of the two sets of inequivalent nuclei in the radical.

2.3.2 General TRIPLE resonance. General TRIPLE resonance gives information on the relative signs of the hyperfine interactions. In order to explain how the experiment works, one needs to consider the energy level scheme for a spin system containing two inequivalent protons (*i.e.*, $S = ½$, $I_1 = ½$, $I_2 = ½$ where $a_1 \neq a_2$) or two nuclei with $I = ½$. The first order energy level diagram, showing the induced transitions and relaxation transitions for this spin system are shown in Fig. 8a for the case where both hyperfine couplings have the same (positive) sign (*i.e.*, $a_1, a_2 > 0$). Fig. 8b shows the corresponding energy level scheme in the case where the hyperfine couplings have opposite signs ($a_1 > 0 > a_2$). For simplicity we will assume an absence of cross relaxation processes (*e.g.*, the $W_{\times i}$ transitions shown in Fig. 7 are neglected). In the first case (Fig. 8a, $a_1, a_2 > 0$), four ENDOR lines are observed arising from the two different NMR transitions in the upper M_S manifold (labelled ν_1^- and ν_2^-) and in the lower M_S manifold (ν_1^+ and ν_2^+). The two ENDOR resonance frequencies for the larger hyperfine coupling a_1 are therefore ν_1^- and ν_1^+. The EPR transition $|-,-,-> \leftrightarrow |+,-,->$, representing the $|M_S,M_I,M_I>$ state, is saturated while the ν_1^+ ENDOR line is simultaneously pumped with one RF field and a second RF field is scanned over the whole range of NMR resonances. In the example shown, ν_1^+ is referred to as the pumping frequency (*i.e.*, the spectral line labelled "pump" in Fig. 8a) while ν_2^- and ν_2^+ are the monitored frequencies. This additional pumping frequency gives rise to intensity changes in the low (ν_2^-) and high (ν_2^+) frequency signals compared to the ENDOR spectrum. From these intensity changes the relative sign of the hyperfine coupling can be determined.

Consider the population difference between the energy levels of the EPR transition ν_{EPR} labelled $|-,-,-> \leftrightarrow |+,-,->$ in Fig. 8a. If the ν_1^+ transition is pumped, whilst monitoring the ν_1^- frequency, the intensity of this ν_1^- line will increase in the general TRIPLE spectrum (indicated by the "up" arrow). This increase occurs for the following reason. The ν_{EPR} transition $|-,-,-> \rightarrow |+,-,->$ is saturated, and the ν_1^- transition $|+,-,-> \rightarrow |+,+,->$ is induced by the second sweeping RF field. Rapid electron relaxation (W_e) occurs from $|+,+,-> \rightarrow |-,+,->$ while the final nuclear transition $|-,+,-> \rightarrow |-,-,->$ (back to the original starting point of $|-,-,->$) is pumped with the saturating ν_1^+ RF field. The nuclear relaxation bottleneck in this circuit is effectively short-circuited by the ν_1^+ pump, and so an increased response occurs in the ν_1^- line. The response of the second monitored ν_2^- transition is more complex. The ν_{EPR} transition $|-,-,-> \rightarrow |+,-,->$ is again saturated, whilst the $|+,-,-> \rightarrow |+,-,+>$ transition is induced by the second ν_2^- RF field. W_e relaxation occurs from $|+,-,+> \rightarrow |-,-,+>$ and finally $|-,-,+> \rightarrow |-,-,->$ is also induced by the second ν_2^+ RF field. However this pathway contains a nuclear bottleneck which is not efficient. A longer but more efficient relaxation pathway is shown in Fig. 9. This pathway or "relaxation loop" gives an increased intensity in the general TRIPLE ν_2^- line compared to the ENDOR spectrum, since it contains all fast electronic relaxation or short-circuited nuclear relaxation processes (note; start at the top left $|-,-,->$ state in Fig. 9 and follow the relaxation pathways with reference to the energy levels in Fig. 8). The remaining ν_2^+ and the pumped ν_1^+ transitions both decrease in intensity (the ν_1^+ line may even disappear) in the general TRIPLE experiment (Fig. 8a). The reason for this is as follows. In the case of the ν_2^+ line the ν_{EPR} transition $|+,-,-> \rightarrow |-,-,->$ is first saturated, the nuclear transition $|-,-,-> \rightarrow |-,-,+>$ is then induced by ν_2^+, W_e then occurs from $|-,-,+> \rightarrow |+,-,+>$ and finally $|+,-,+> \rightarrow |+,-,->$ is induced by ν_2^-. But the population difference between the levels ν_2^+ are already reduced by the saturating and competing ν_1^+ field, therefore a smaller ENDOR response is observed (the line decreases, indicated by the "down" arrow). Finally for the pumped line ν_1^+, the population difference in the levels $|-,-,-> \leftrightarrow |-,+,->$ is significantly reduced by the saturating ν_1^+ transition, so the ENDOR response is severely diminished. The most important point to note from all of the above trends, is that transitions arising from the same M_S manifold behave in the same way in the general TRIPLE experiment; the sign of the hyperfine coupling determines which M_S manifold a given transition falls into. Therefore, if two couplings behave in the same way, they have the same sign.

The energy level scheme for the case where the hyperfine couplings have unequal signs ($a_1 > 0 > a_2$) is shown in Fig. 8b. It is important to note that the high and low frequency transitions now show up in both M_S states in a mixed fashion. Consider once again the intensity changes to the ENDOR signals by pumping the ν_1^+ transition. If the pumping and monitoring frequencies are irradiated in the same M_S manifold, a decrease in intensity of the lines is expected since the relaxation loop can only be closed by including W_n processes (which are less effective than W_e). As shown in Fig. 8b, ν_1^+ and ν_2^- are both in the same lower M_S manifold, and both lines decrease in intensity. As before, an increase in intensity is expected when the pumping and monitoring frequencies are in different M_S manifolds (ν_1^- and ν_2^+). To summarise, if one nucleus has the same sign as the pumped nucleus, the intensity changes of their respective ENDOR lines behave in the same way in a general TRIPLE resonance experiment (and *vice versa* if they have opposite signs).

As an example, the general TRIPLE resonance experiment for the phenalenyl radical is shown in Fig. 5. From the line intensity patterns it is clear that one low frequency line is enhanced, while the other is diminished, when pumping a high frequency transition. Therefore, the low frequency lines belong to different M_S manifolds, so that the two hyperfine couplings have opposite signs.

3 Orientation selective ENDOR; structure determination in frozen solution

All of the preceding discussions have only considered the ENDOR spectra for organic radicals in isotropic solution. In frozen solution, or in polycrystalline media, all orientations of the paramagnetic species are observed, and one thus obtains an anisotropic EPR spectrum, particularly for transition metal species. The ENDOR spectra of such systems are consequently

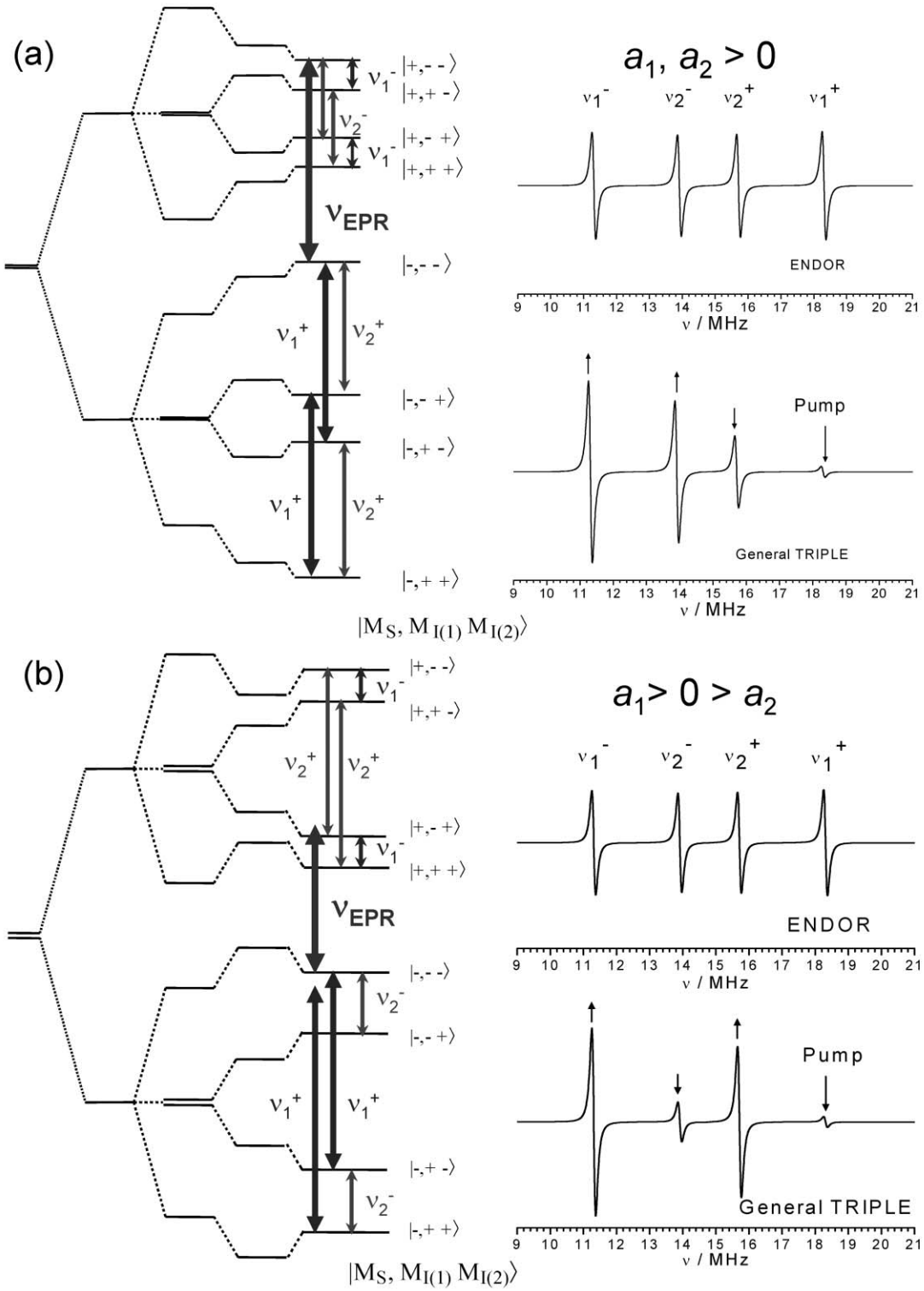

Fig. 8 Energy level diagram for a three spin system ($S = ½$ and two inequivalent $I = ½$ nuclei such that $a_1 \neq a_2$) in the case where (a) both couplings have the same sign ($a_1, a_2 > 0$) and (b) where both couplings have opposite signs ($a_1 > 0 > a_2$). The induced EPR (ν_{EPR}) and pumped NMR (ν_1^+) transitions are labelled with the thick solid arrows. The ENDOR and resultant general TRIPLE resonance spectra are also shown.

more complex, requiring a detailed understanding of the ***g*** and ***A*** anisotropy of the system. In the following discussions, the basic concepts of interpreting anisotropic (polycrystalline) EPR spectra will not be discussed (as this is presented in many of the cited textbooks and reviews). Instead we will devote our attention to a description of the interpretation of powder

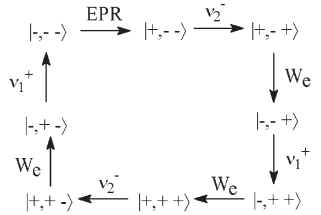

Fig. 9 Relaxation loop responsible for the enhanced intensity of the ν_2^- line in the general TRIPLE spectrum (shown in Fig. 8a) for the hypothetical system $S = ½$, $I_1 = ½$, $I_2 = ½$ where a_1, $a_2 > 0$.

ENDOR spectra, and how analysis of these spectra can yield structural information.

The determination of the structural parameters, such as the distance and direction of a spin active nucleus from a paramagnetic centre, using ENDOR spectroscopy first requires a knowledge of the ENDOR resonance condition in the solid state. The expression, given in eqn (9) above for isotropic systems, is not suitable for this and a more complete resonance condition (discussed below) which considers all of the anisotropies in the $\boldsymbol{g}$ and $\boldsymbol{A}$ tensors is required. Unfortunately it is not particularly easy to determine the form of the powder ENDOR spectrum, even for simple systems, simply by inspection of a solid state resonance expression. This is not a particular problem in practice, as there are few real systems that give rise to simple ENDOR spectra which can be analysed by visual inspection and a simulation of the powder ENDOR spectrum is therefore necessary.

3.1 Simulation of powder ENDOR spectra

The concept of ''angular selective'' or ''orientation selective'' ENDOR by saturation of selected turning points in an EPR spectrum, yielding single crystal like spectra from polycrystalline matrices, was first proposed by Rist and Hyde,[21] and further developed by Hoffman[9] and Kreilick.[10] Before analysing the ENDOR spectra, the $\boldsymbol{g}$ tensor orientations contributing to the EPR resonance positions at the selected magnetic field $\boldsymbol{B}_0$ in the orientation selective ENDOR experiment must first be determined. The EPR spectrum is treated as a superposition of resonances from randomly orientated molecules, so that the applied field ($\boldsymbol{B}_0$) adopts all possible orientations with respect to the chosen molecular frame as it is swept. The ENDOR spectra are then recorded at fixed magnetic fields, so that the response from a polycrystalline sample arises only from the subset of molecules having orientations that contribute to the EPR intensity at that particular $\boldsymbol{B}_0$ field. The EPR resonance positions $\boldsymbol{B}_r$ for given (θ,$\boldsymbol{\phi}$) orientations are expressed to first order as:

$$B_r = \left[\frac{h\nu - m_I A(\theta,\phi)}{\mu_B g(\theta,\phi)}\right] \tag{14}$$

where ν is the microwave frequency, m_I the magnetic spin quantum numbers, and the other symbols have their usual meaning. In practice, either a second order or an exact expression is required when the magnitude of the hyperfine coupling is significant, as is often the case in transition metals. The terms $\boldsymbol{A}(\theta,\boldsymbol{\phi})$ and $\boldsymbol{g}(\theta,\boldsymbol{\phi})$ in eqn (14) may be obtained from eqns (15) and (16) as follows;

$$A(\theta,\phi) = \left[\sum_{i=1}^{3}\left[\left(\sum_{j=1}^{3} g_j h_j A_{ji}\right) - h_i \nu_N\right]^2\right]^{1/2} g(\theta,\phi)^{-1} \tag{15}$$

$$g(\theta,\phi) = \left[\sum_{i=1}^{3} (g_i h_i)^2\right]^{1/2} \tag{16}$$

where h_i are the direction cosines ($h_1 = \cos\boldsymbol{\phi}\,\sin\theta$, $h_2 = \sin\boldsymbol{\phi}\,\cos\theta$ and $h_3 = \cos\theta$). The angles θ and $\boldsymbol{\phi}$ are field orientation parameters in the g frame, where θ represents the angle between g_z and $\boldsymbol{B}_r$, and $\boldsymbol{\phi}$ between g_x and the projection of $\boldsymbol{B}_r$ in the x–y plane. Thus, the resonance fields for each m_I state may be calculated for different sets of (θ, $\boldsymbol{\phi}$) orientations. Note, that for *non-axial* systems different combinations of (θ,$\boldsymbol{\phi}$) may have the same resonant field and thus it is not possible to determine (θ,$\boldsymbol{\phi}$) knowing $\boldsymbol{B}_r$. The resonant fields thus obtained are convolved with a lineshape function (Gaussian) to obtain their intensity at the magnetic field ($\boldsymbol{B}_0$), used for the ENDOR experiment, and the transition frequencies for each nucleus calculated using the following ENDOR resonance expression for the solid state (eqn (17)):

$$\nu_\pm = \left[\sum_{i=1}^{3}\left[\frac{m_s}{g_{(\theta,\phi)}}\left(\sum_{j=1}^{3} g_j h_j A_{ji}\right) - h_i \nu_N\right]^2\right]^{1/2} \tag{17}$$

where h_i are the direction cosines of $\boldsymbol{B}_r$ in the molecular axis system, A_{ji} is the orientation dependent value of the hyperfine coupling, ν_n is the nuclear Larmor frequency and m_S the spin quantum number. Since the intensity of the ENDOR lines is proportional to the transition probability of the nuclear transitions, an appropriate expression must be added to deal with this term. However, for convenience we have set the transition probability to 1. Finally an appropriate lineshape function may be convolved onto the ENDOR resonance frequencies obtained. The ENDOR spectra are then simulated at the different field positions, providing information on the principal components of the various hyperfine tensors as well as their orientation relative to $\boldsymbol{g}$. This tensor, is then analysed to extract the isotropic and anisotropic (or dipolar) contributions. The latter contribution is used to determine the distance to the interacting nucleus using the simple point dipole approximation, discussed further in section 3.2:

$$A_{dip}^{\xi} = \left(\frac{\mu_0}{4\pi h}\right)\frac{g\mu_\beta g_N \mu_N}{R^3}\left(3\cos^2\xi - 1\right) \tag{18}$$

Having explained how to simulate the ENDOR spectrum arising from a disordered system, we shall now continue by explaining the form of the ENDOR spectrum for a number of model systems, and how the parameters obtained from this may lead to the determination of three dimensional molecular structure. In order to specify the position of an object in a three dimensional space, three pieces of information are required: an origin; a distance from that origin; and a direction. For the purposes of this discussion, the origin of our coordinate system is taken to be the position of a localised,

unpaired electron on a molecule. Clearly, many paramagnetic systems contain delocalised electron spins and whilst these are not discussed here, they are nevertheless amenable to study using this approach.

3.2 Determination of direction

The determination of the direction from an unpaired electron to a spin active nucleus is based upon the principle of magnetic angle selection which, in turn, relies upon the anisotropy inherent in the EPR spectrum and the selectivity of the ENDOR technique, as discussed above. The EPR spectrum from a paramagnetic system in a disordered matrix comprises the sum of the spectra from the individual paramagnets in the system. Thus, for a given magnetic field value $\boldsymbol{B}_0$, only those paramagnets which are on resonance at that particular field contribute to the EPR spectrum and, by extension, to the ENDOR spectrum acquired at that magnetic field setting.

The simplest system is one in which the anisotropy in the EPR spectrum is very small, such that the spectrum is effectively isotropic (for example at X-band frequencies). In this case all orientations of the paramagnet are selected for a given $\boldsymbol{B}_0$ field and we obtain a true powder type, anisotropic, ENDOR spectrum with features corresponding to the principal values of the hyperfine tensors for the spin active nuclei in the system (some examples are given in section 4). Additionally it is not possible to use such systems to determine direction, and the observed ENDOR spectrum does not change as the magnetic field is moved across the EPR spectrum (in systems where the anisotropy is low, a different ENDOR spectrum may be obtained from the wings of the EPR spectrum compared to the spectrum at the centre). However, it must be stressed that increased g-value resolution can be obtained at higher frequencies (35 GHz, 95 GHz and higher), allowing orientation selective ENDOR experiments to be performed.

If we consider a system with an axial $\boldsymbol{g}$-tensor, no hyperfine interaction and an infinitessimal EPR linewidth then, by setting the magnetic field $\boldsymbol{B}_0$ such that it corresponds to the $g_\parallel$ feature in the EPR spectrum, we will record an ENDOR spectrum from only those paramagnets which have their highest order symmetry axis (which corresponds to the $g_\parallel$ direction) parallel to the applied magnetic field. Similarly, by moving the magnetic field to the $g_\perp$ feature at other end of the EPR spectrum, we obtain an ENDOR spectrum comprising only those paramagnets with their highest order symmetry axis perpendicular to the applied magnetic field.

In practice, however, rather than thinking of paramagnets aligned with an external magnetic field of fixed direction, it is easier to consider the paramagnets to be fixed and the magnetic field as a vector within the g-frame, as shown in the inset in Fig. 10. Thus it is clear that for a magnetic field corresponding to the $g_\parallel$ position in the EPR spectrum, the angle θ equals 0° and for the perpendicular position, θ equals 90°. At a magnetic field position between these two extremes we obtain a value of θ somewhere between 0° and 90° (see Fig. 10); the exact value of θ may be obtained from eqn (19);

$$\theta = \cos^{-1}\left[\frac{g_\theta^2 - g_\perp^2}{g_\parallel^2 - g_\perp^2}\right]^{1/2} \qquad (19)$$

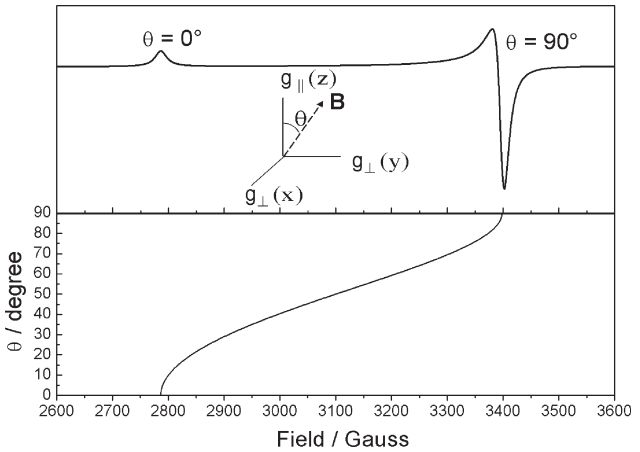

Fig. 10 Angular distribution in the EPR spectrum of an axial paramagnet with no hyperfine interaction (at X-band frequencies). A definition of the magnetic field direction (θ) for an axial paramagnet ($g_\parallel$,$g_\perp$) with no hyperfine interaction is shown in the inset.

where g_θ is the g-value for the angle θ corresponding to the set magnetic field position. Whilst not explicitly discussing lower symmetry (rhombic systems) in this section, it is worth noting that for these systems it is necessary to define a second angle in the perpendicular plane, where $\boldsymbol{\phi}$ = 0° corresponds to the x direction of a right handed coordinate system, thus giving rise to the term $g_{\theta,\boldsymbol{\phi}}$ in eqn (15); in an axial system all values of $\boldsymbol{\phi}$ are equivalent.

It is important to note at this point that the θ = 0° direction in this case corresponds to a single unique direction and thus gives rise to an ENDOR spectrum corresponding to that one direction, often referred to as a "single crystal" type spectrum (in practice this is not entirely true as the EPR linewidth results in the selection of a range of theta values). Any angle of θ other than this in an axial system results in a restricted set of orientations, due to the equivalence of $\boldsymbol{\phi}$ in the perpendicular plane; one may visualise this selection by imagining the magnetic field vector precessing about the parallel direction. The implication of the equivalence of $\boldsymbol{\phi}$ in an axial system for structure determination is that we can only specify the direction in terms of the angle θ. This may in fact be advantageous as the loss of some spatial information is offset by a simplification of the analysis, as we shall see. Thus, having discussed how the magnetic field may be used to select a particular direction, the next step is to determine what effect this will have on the resulting ENDOR spectrum.

The simplest system we might envisage is the EPR system described above coupled to a single proton whose axial hyperfine tensor is oriented in the same way as the electronic $\boldsymbol{g}$-tensor. In this case, setting the magnetic field to the parallel or perpendicular feature in the EPR spectrum selects the parallel or perpendicular component of the hyperfine tensor respectively and any intermediate position selects the equivalent angle in the hyperfine tensor. Thus, for the parallel position in the EPR spectrum we expect to see an ENDOR spectrum comprising a pair of lines of separation $A_\parallel$. As the magnetic field is moved across the EPR spectrum these lines will move closer together, according to θ, until at $g_\perp$ their

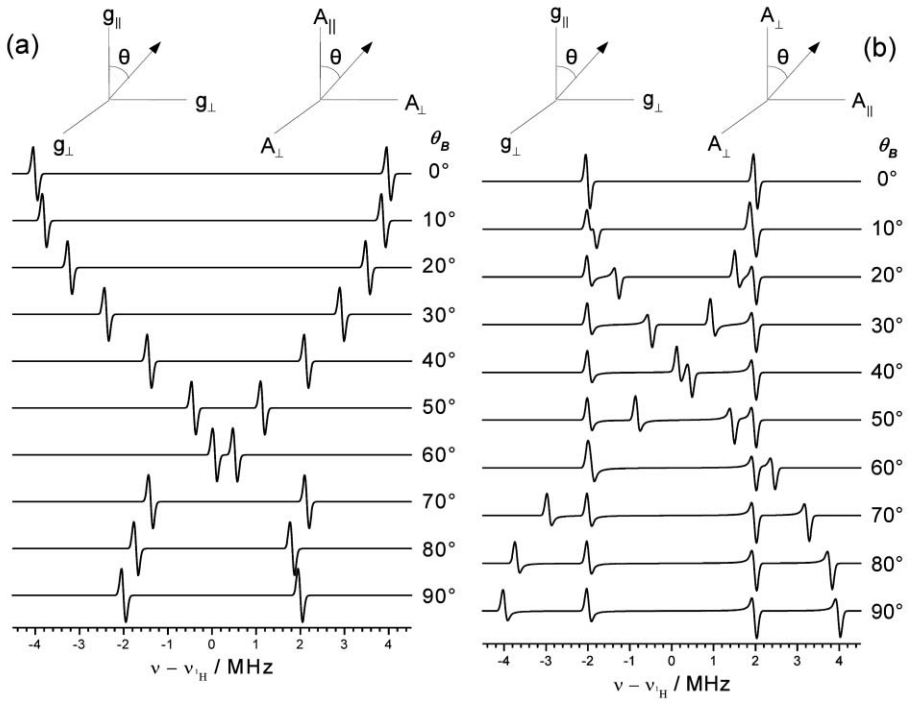

Fig. 11 Magnetic field orientation (θ) dependence of the ENDOR spectrum, simulated for an axial EPR system with no hyperfine interaction, for a proton (a) with its purely dipolar hyperfine matrix coincident with the g matrix, and (b) with the parallel component of its purely dipolar hyperfine matrix in the perpendicular plane of the ***g***-matrix. Note how the peaks cross the centre of the spectrum due to the difference in signs between the parallel and perpendicular dipolar hyperfine interactions. A definition of the axial system in which the g and hyperfine matrices are (a) coincident and (b) mutually perpendicular is also shown.

separation will correspond to $A_{\perp}$. These trends are illustrated in the simulated ENDOR profiles shown in Fig. 11a.

The next simplest case is to consider the above system but with the proton hyperfine tensor oriented at right angles to the ***g***-tensor, such that $g_{\|}$ corresponds to $A_{\perp}$ as shown in Fig. 11b. It is thus apparent from this figure that setting the magnetic field to the $g_{\|}$ feature will produce an ENDOR spectrum of just two lines separated by $A_{\perp}$. At a field position corresponding to $g_{\perp}$, however, things are more complicated as both $A_{\|}$ and $A_{\perp}$ lie in the $g_{\perp}$ plane and, indeed we observe four lines in the ENDOR spectrum, two for each coupling. This ENDOR spectrum is, therefore, a powder type spectrum arising from a restricted set of orientations.

When selecting angles of θ other than 0° and 90°, a little more thought is required. Clearly we are going to select a value A_{θ} somewhere between $A_{\perp}$ and $A_{\|}$ but we may also note (using the idea of a precessing magnetic field vector) from Fig. 11b that for every angle of θ the magnetic field vector intersects the $A_{\perp}$ plane. Hence, as we move the magnetic field from $g_{\|}$ to $g_{\perp}$ we see a pair of lines corresponding to $A_{\perp}$, from which a second pair of lines split and move to $A_{\|}$. It is worth noting, that for a predominantly dipolar hyperfine interaction, $A_{\|}$ and $A_{\perp}$ have opposite signs (see below) and thus will cross the centre of the ENDOR spectrum on moving the magnetic field from to $g_{\|}$ to $g_{\perp}$ as seen in Fig. 11b. As a result of this, they will appear to have a different lineshape to those arising from a hyperfine tensor with a large isotropic component. It is useful to note that a proton with its (axial) hyperfine tensor principal axes non-coincident with the g tensor axes creates a further reduction in symmetry and more than four lines may be observed for a single proton in the ENDOR spectrum

3.3 Determination of distance

The determination of electron–nuclear distance from ENDOR spectroscopy relies upon the point dipole approximation (see eqn (18)) which considers the through-space magnetic interaction between two magnetic dipoles. The equation as it stands enables the distance (R) in metres to be determined for a pure dipolar coupling for a given orientation (θ) of the hyperfine tensor in Hz (μ_0 is the vacuum permittivity, μ_N and μ_B are the nuclear and Bohr magneton respectively, g and g_N are the electronic and nuclear g values and h is Planck's constant). In practice the hyperfine tensor is determined by simulation of the ENDOR spectrum and the parallel dipolar component ($\theta = 0°$) used for convenience. It may also be observed from eqn (16) that the dipolar coupling for $\theta = 90°$ is $-½$ times that for $\theta = 0°$. The point dipole approximation as it is given here is only valid for distances greater than 2 Å[18] a situation common for transition metal complexes, in which regime it is extremely good. It should also be noted that there is often an isotropic component to the hyperfine coupling which must first be subtracted to yield the pure dipolar hyperfine tensor.

3.4 The method in practice; a simple example in frozen solution

The ENDOR spectrum for the $[VO^{IV}(H_2O)_5]^{2+}$ system, obtained simply by dissolving vanadyl sulphate in water, may be analysed using the methods described above. The EPR

spectrum of this system (not shown) is purely axial at X-band with the unpaired electron predominantly localised on the vanadium atom and the parallel direction corresponds to the V=O bond. The structure of the complex may be simplified for the purposes of the analysis as follows. First, the inability to discriminate between directions in the perpendicular plane means that the four equatorial molecules are indistinguishable (Fig. 12a). Second, for simplicity the two protons on each water molecule may be assumed to be magnetically equivalent and, thus each water molecule may be considered a single proton. Finally, it may be assumed that the proton hyperfine interaction is purely dipolar (simulations have shown that this is a valid assumption), and the maximum ($A_{\|}$) component is along the VO–H direction. Thus the problem is reduced to two protons, one in each of the two situations described above (see Fig. 12b).

The ENDOR spectra (Fig. 12c) taken with the magnetic field set to the parallel and perpendicular directions in the EPR spectrum may be assigned as follows. The ENDOR spectrum corresponding to $\theta = 0^{\circ}$ should contain only the parallel component of the hyperfine coupling to the axial proton and the perpendicular component of the equatorial proton. Indeed two sets of features are observed, one with a coupling of 6.3 MHz and the other with a coupling of (−)4.4 MHz. The latter coupling also appears in the spectrum recorded at θ = 90°, and as such may be assigned to $A_{\perp}$ for the equatorial protons; hence the 6.3 MHz coupling may be assigned to $A_{\|}$ for the axial protons.

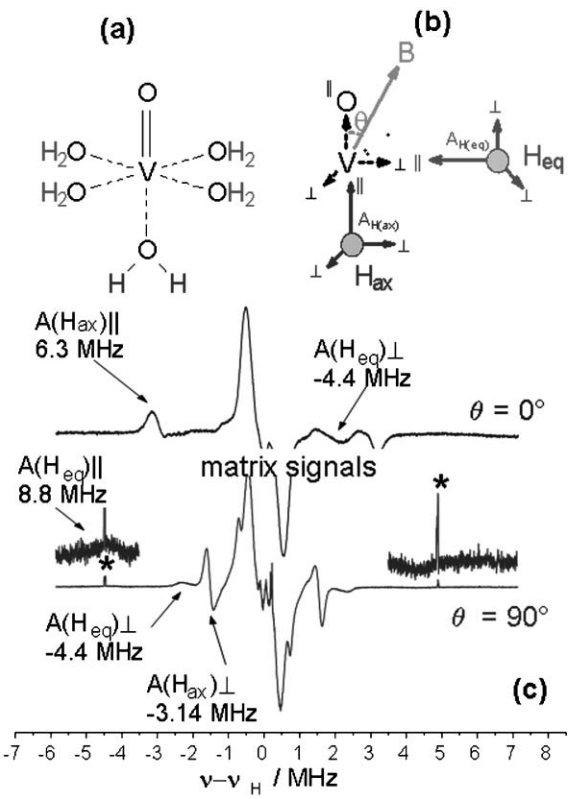

Fig. 12 (a) Schematic illustration for the structure of the $[VO^{IV}(H_2O)_5]^{2+}$ complex, and (b) the reduced structure for simplification of the ENDOR analysis. (c) Experimental ^{1}H ENDOR spectra of $[VO^{IV}(H_2O)_5]^{2+}$ recorded at 10 K at positions in the EPR spectrum corresponding to the parallel ($\theta = 0^{\circ}$) and perpendicular ($\theta = 90^{\circ}$) directions. The sharp features marked * are instrumental artefacts.

Assuming a purely dipolar interaction (which, as it turns out in this case, is a good assumption) between the protons and the electron, we should expect to observe in the spectrum recorded at $\theta = 90^{\circ}$, according to eqn (16), a coupling of 8.8 MHz corresponding to $A_{\|}$ for the equatorial protons; a coupling of (−)3.15 MHz corresponding to $A_{\perp}$ for the axial protons; and the (−)4.4 MHz coupling described above. It may be seen from Fig. 12 that these couplings are indeed observed as predicted, that they are purely dipolar and thus using the $A_{\|}$ components, distances of 2.90 Å and 2.61 Å from the vanadium centre may be obtained for the axial and equatorial protons respectively.

4 Examples of solution and powder ENDOR measurements

In the following section, a series of examples will be given to illustrate how structural information about a paramagnetic species can be obtained through analysis of the ENDOR spectrum. The first two examples 4.1–4.2 will demonstrate the type of information available from solution (isotropic) ENDOR spectra, primarily from organic radicals. The remaining examples 4.3–4.8 will demonstrate the applications of orientation selective ENDOR for determination of structural parameters in polycrystalline media or disordered matrices. While some of these latter examples include pulse ENDOR measurements, as opposed to cw-ENDOR, the stragety for analysing and simulating the field dependent ENDOR spectra are essentially similar to the principles outlined in Section 3 above. Examples 4.3–4.8 below are divided into two general categories. In examples 4.3–4.4, the ***g*** or ***A*** anisotropy is small so that the vast majority of the molecular orientations are selected simultaneously, resulting in a ''true'' powder type ENDOR spectrum. In examples 4.4–4.8, the EPR spectra are dominated by large ***g*** or ***A*** anisotropies so that ''single-crystal'' like ENDOR spectra are obtained by setting the magnetic field at so-called turning points in the EPR spectra where ***g*** or ***A*** anisotropy is evident.

4.1 Secondary radical discrimination in mixed radical systems

The reaction of 2,3-dimethylhydroquinine with sodium methoxide produces the expected 2,3-dimethyl-1,4-benzoquinone anion radical, whose structure and EPR spectrum is presented in Fig. 13. The EPR spectrum for this species is based on a simple triplet of septets arising from the set of two equivalent protons in the 5,6 positions on the aromatic ring and the six equivalent methyl protons. This solution EPR spectrum may therefore be readily assigned to the 2,3-dimethyl-1,4-benzoquinone anion radical. However, careful inspection of the EPR spectrum, also shows that it contains a number of low intensity signals from a second paramagnetic species. From this EPR spectrum it is possible, by careful positioning of the magnetic field, to obtain an ENDOR spectrum which essentially comprises signals from the second, unassigned species alone. This ENDOR spectrum (shown in Fig. 13) appears to contain just three pairs of lines, but the increased resolution of the

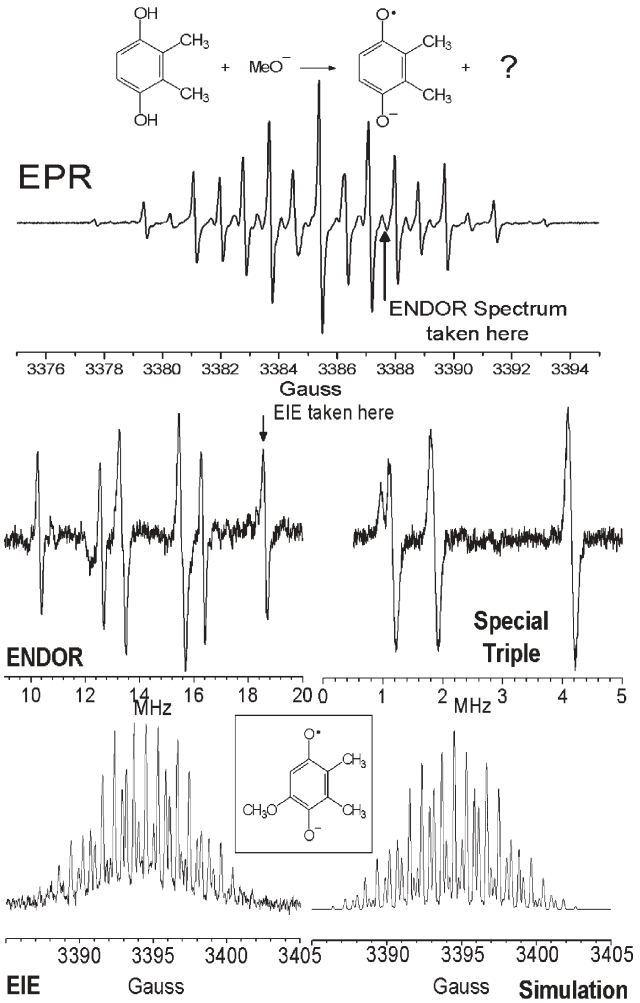

Fig. 13 cw-EPR spectrum of the primary 2,3-dimethyl-1,4-benzoquinone anion radical obtained by reaction of 2,3-dimethylhydroquinone (0.1 M) with sodium methoxide (0.01 M). The associated ^{1}H ENDOR, special TRIPLE resonance, ENDOR Induced EPR and EIE simulation of the secondary 2,3-dimethyl-5-methoxy-1,4-benzoquinone anion radical are also shown. All spectra were recorded in methanol at 230 K.

special TRIPLE spectrum shows that the innermost pair of lines comprises two couplings. In addition, the special TRIPLE spectrum (shown in Fig. 13) was used to show that the intensity ratio of these four sets of lines were 1 : 3 : 3 : 3.[22] By monitoring the intensity of one of the ENDOR lines as a function of magnetic field, the ENDOR-induced-EPR spectrum (EIE) may be obtained (Fig. 13). This spectrum is obtained in absorption mode (for technical reasons) and it represents the EPR spectrum of the second unassigned species alone, even though it was obtained from the reaction mixture. This EIE spectrum was successfully simulated based on the hyperfine couplings (*ex* ENDOR) and multiplicities (*ex* special TRIPLE), and assigned to the 2,3-dimethyl-5-methoxy-1,4-benzoquinone anion radical.[22] The relative signs of the couplings were also obtained from the general TRIPLE spectrum (not shown) and compared with the results of molecular orbital calculations for additional confirmation. The splitting constants for this anion radical (with their relative signs) were therefore found to be: a_H(H) = −2.1 MHz, a_H(CH_3) = 8.372 MHz, a_H(CH_3) = 3.752 MHz and a_H(OCH_3) = 2.324 MHz.[22] This simple example illustrates how the range of ENDOR and TRIPLE resonance experiments can be collectively employed to ascertain the structure of organic radicals, even in cases where minor secondary radical species may be present.

4.2 Electron delocalisation in conducting organic materials

Understanding the mechanism of electron transport in conducting polymers requires information about how the electrons are delocalised along the conjugated π systems of the polymer chains and how extensively electron hopping between adjacent polymer chains contributes to conduction.[23] Since EPR and ENDOR can reveal information on the magnitude of the electron–nuclear interactions, through the hyperfine couplings, the amount of electron delocalisation in conducting polymers can be conveniently probed. Model systems representing the structural subunits of a polymer like phenylenediamine were investigated,[23] with various substituents attached to the chain to probe the physicochemical modifications of chain substituents and chain length on electron delocalisation. EPR, ENDOR and TRIPLE resonance spectrospcopy of the radical cations in solution provided detailed information on the hyperfine couplings which were compared to density functional theory (DFT) calculations. The solution EPR and ENDOR spectra of the radical cation of the mono-*N*-phenyl substituted dimer is shown in Fig. 14. The EPR spectrum is dominated by interactions to two equivalent ^{14}N nuclei (0.55 mT) and two equivalent N–H protons (−0.613 mT). The remaining proton interactions were identified and assigned as $H_{2,3,5,6}$ = −0.154, H_{para} = −0.183, H_{ortho} = −0.103 and H_{meta} = 0.046 mT. While the EPR spectrum was well resolved, the simulation of its complex profile was significantly aided by the ENDOR spectrum which provided the hyperfine couplings directly in frequency units. The ^{14}N coupling and the larger N–H couplings are clearly visible in the ENDOR spectrum, while the smaller couplings to the more remote protons of the phenyl groups were easily extracted, illustrating the power of ENDOR to simplify the analysis of complex EPR spectra. These results lead to the conclusion that in all the model systems studied, the spin and charge were essentially confined to the central phenylenediamine moiety, with only a very limited degree of electron delocalisation into the adjacent phenyl substituents. In other words, the conducting properties of polyanilines arise predominantly by three dimensional charge hopping between the adjacent polymer chains, rather than by one dimensional solitary conducting chains.

4.3 Spin density distributions in a thiazyl-based organic ferromagnet

Many dithiadiazolyl radicals can associate to form spin-paired dimers in the solid state. By comparison a number of perfluorophenyl derivatives, such as *para*-$O_2NC_6F_4CNSSN$, retain their free radical nature in the solid state and this particular radical was found to undergo ferromagnetic

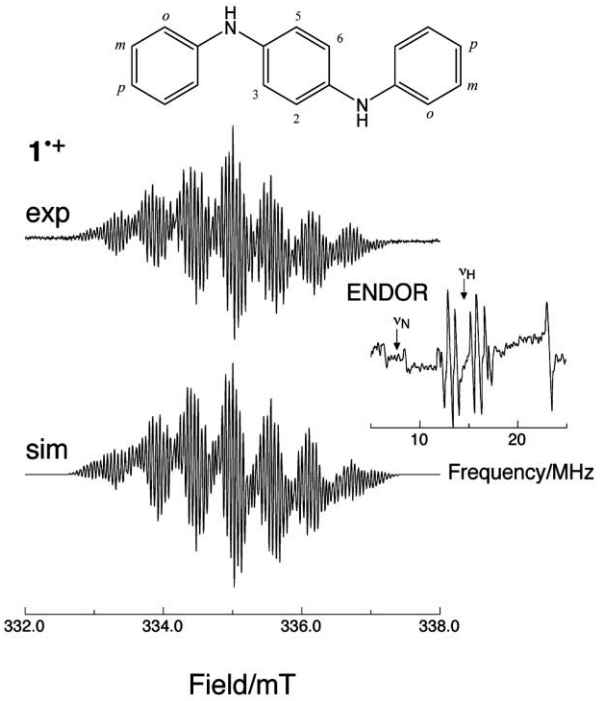

Fig. 14 cw-EPR and ^{1}H ENDOR solution spectra, and associated simulation, of the radical cation of the mono-*N*-phenyl substituted dimer (structure shown above). Reproduced with permission from reference 23, © 2004 American Chemical Society.

ordering below 1.3 K.[24] Subtle structural changes to these radicals can lead to new magnetically ordered systems, so that it is extremely important to probe the spin density and charge density distribution within these radicals. X- and Q-band EPR spectra (Fig. 15) of *para*-$O_2NC_6F_4CNSSN$ exhibited well resolved hyperfine couplings to the two N atoms of the heterocyclic dithiadiazolyl ring and smaller superhyperfine couplings to the two *ortho*-^{19}F atoms of the phenyl substituents (see radical structure in Fig. 15). The hyperfine couplings (A_1, A_2, A_3) were determined as (39, $\pm$2.5, $\pm$2.5) MHz for ^{14}N and ($\sim$9, $\sim$5, $\sim$5) MHz for ^{19}F indicating that while the spin distribution is predominantly localised on the N and S atoms of the heterocyclic ring, a small spin density is present in the perfluorophenyl ring. The orientation selective ^{19}F ENDOR spectra were subsequently recorded at both X- and Q-band frequencies, at field positions close to the principle turning points in the spectra (shown in the EPR spectrum in Fig. 15). The Q-band ENDOR spectra were less complicated, compared to X-band, as fewer orientations are selected at the chosen field positions. Both the large *ortho*-^{19}F coupling and the smaller *meta*-^{19}F coupling were visible as separate pairs of lines in the ENDOR spectra measured at positions 1 and 3 (I = ½ for ^{19}F). By comparison, the powder ENDOR pattern at position 2, shows more than one orientation to the ^{19}F interaction, so more lines are visible.[25] Analysis of these ENDOR spectra revealed the ^{19}F hyperfine tensors of (A_1, A_2, A_3) = (11.4, $\pm$3.5, $\pm$3.5) MHz for *ortho* ^{19}F and (1.0, $\pm$0.19, $\pm$0.4) MHz for *meta*-^{19}F suggesting spin densities of 10^{-3} and 10^{-4} magnitude respectively for the F atoms *ortho*- and *meta*- to the dithiadiazolyl ring.

4.4 Spin density distributions in cycloheptatrienylmolybdenum complexes

The redox chemistry of the complexes based on metal phosphine auxiliaries such as $ML_2(\eta\text{-}C_5R_5)$, where M = Fe or Mo, L = PPh_3 and L_2 = dppe, has attracted significant attention in recent years. In particular a series of cycloheptatrienyl molybdenum auxilary $MoX(dppe)(\eta\text{-}C_5R_5)$ derivatives, where X = I, Br, Cl, F, NCS, CN, *etc.*, were synthesised and studied by cyclic voltammetry for the reversible one electron oxidation to the corresponding 17-electron radicals.[26] The distinctive features of these cycloheptatrienyl–molybdenum systems are the ease of one electron oxidation to the corresponding 17-electron radical cations $[MoX(dppe)(\eta\text{-}C_7H_7)]^+$, the stability of these radicals and the well resolved nature of the solution EPR spectra. Calculations to determine the contributions to the ground state molecular orbital from the *n*s orbital of the ligand X was possible *via* the EPR spectra, but the higher resolving power of ENDOR was required to obtain this information on the dppe phosphorus s and p orbitals.[26] In frozen solution, the complex $[MoF(dppe)(\eta\text{-}C_7H_7)]^+$ exhibits a small g anisotropy with g_1 = 2.008, g_2 = 1.988 and g_3 = 1.955 as compared to the EPR linewidth (Fig. 16). By setting the magnetic field to a position corresponding to the centre of the EPR spectrum, a complete set of molecular orientations corresponding to all principal values of the local hyperfine tensors is selected. Indeed, a true powder type ENDOR spectrum is obtained at 10 K (Fig. 16) and demonstrates clearly that, for this particular complex, the phosphorus hyperfine tensor is axial having couplings of $A_\perp(^{31}P)$ = 61.9 MHz and $A_\parallel(^{31}P)$ = 68.4 MHz.[26] In common with all such systems, the directional information regarding the position of the phosphorus atom with respect to the molybdenum centre was not available in this case but, nevertheless, these spectra assist in the characterisation of these species. In addition, calculations using the above data suggest that, for these types of complexes, the contributions to the ground state molecular orbital from phosphorus are small and that the unpaired electron, in the most part, resides in a predominantly metal-based molecular orbital.

4.5 Detection of a nitrogenase catalytic intermediate

Biological nitrogen fixation is catalysed by the enzyme nitrogenase, which is based on two component proteins; the MoFe protein and the Fe protein. This enzyme catalyses not only N_2 reduction, but also the reduction of other triply bonded substrates such as alkynes. While the FeMo-cofactor is known to provide the site for substrate reduction, the intermediates of the substrate derived species and the structure of the site containing the bound substrate remains uncertain. Using ^{13}C labelled propargyl alcohol ($H^{13}C_3{\equiv}^{13}C_2{-}^{13}C_1H_2OH$) as substrate, a reaction intermediate was trapped in which the S = 3/2 spin state of the FeMo-cofactor was converted to an S = ½ spin state.[27] ^{13}C ENDOR of the intermediate showed three well resolved ^{13}C doublets (I = ½ for ^{13}C) indicating the presence of a C_3 molecule bound to the FeMo-cofactor. Pulsed ENDOR measurements at a selected field position in the EPR spectrum showed the presence of two intense doublets centred on ν_n for ^{13}C. By

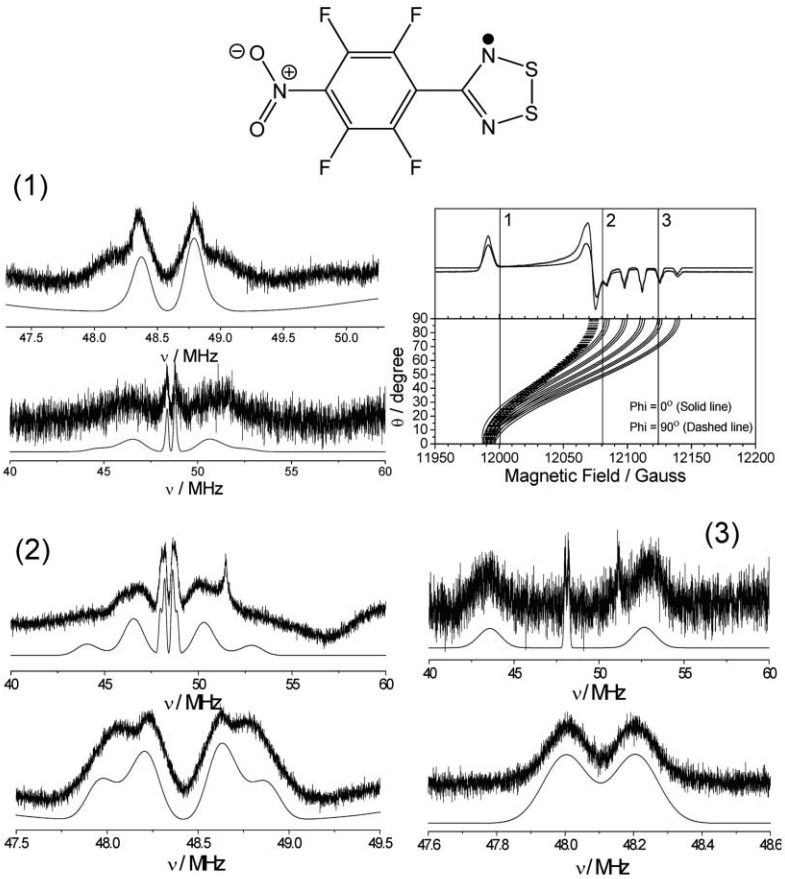

Fig. 15 cw-Q-band ^{19}F ENDOR spectra of a *p*-$O_2NC_6F_4CNSSN$ organic ferromagnet, recorded at different field positions in the EPR spectrum (shown in the top right hand corner). The ENDOR spectra are shown over a wide and narrow sweep at each field position, to highlight the large and small ^{19}F couplings.

lengthening the τ time in the refocussed four pulse MIMS ENDOR measurement, an increase in sensitivity to couplings with smaller A_{13C} values can be achieved. In this way, the pulsed ENDOR measurements unambiguously identified the presence of three distinct and different ^{13}C nuclei. The ^{13}C hyperfine tensor was subsequently determine by analysis of the orientation selective *cw* and pulsed ENDOR spectra (shown in Fig. 17) yielding the hyperfine tensors of (A_1, A_2, A_3) = (5.1, 2.4, 3.5) MHz for $^{13}C_3$, (0.55, 1.3, 1.4) MHz for $^{13}C_2$ and (0.24, 0.6, 0.4) MHz for $^{13}C_1$. The $^{1,2}H$ hyperfine tensors were also determined from the 2D field frequency ENDOR spectra, and combined with the ^{13}C tensors, the authors were able to propose a model structure for the intermediate based on a novel bio-organometallic complex in which a reduction product of the propargyl alcohol binds as a metallacyclopropane ring to a single Fe atom on the FeMo-cofactor. This detailed paper[27] illustrates very elegantly the advantages of combining cw- and pulsed ENDOR measurements for systems where single crystals are difficult to obtain.

4.6 Observation of enantiomer epoxide discrimination by metal complexes

The ability to observe and quantify the weak diastereomeric interactions between chiral species in solution is fundamentally important for the mechanistic understanding of enantioselective separations and chemical transformations. While a number of techniques can detect the presence of different diastereomeric states, few techniques can characterise the *structural* differences in the spatial orientation of the chiral complex, particularly in solution and in cases where the chiral interaction is very weak. It was shown for the first time,[28] how ENDOR spectroscopy could be used to structurally characterise the very weak interaction between a chiral paramagnetic metal complex (*S*,*S* or *R*,*R*)-[VO(**1**)]-*N*,*N*′-bis(3,5-di-*tert*-butylsalicylidene)-1,2-cyclohexanediamino vanadium(IV) oxide and a chiral epoxide (*R*- or *S*-) propylene epoxide (Fig. 18). DFT calculations revealed that the binding energy between the epoxide and the metal complex was less than 10 kJ mol^{-1}, suggesting that the difference in energy between the enantiomeric pairs ($\Delta\Delta G$) must be extremely small indeed. Nevertheless, it was possible to discriminate subtle differences in the ^1H ENDOR spectra of the bound epoxides (peaks labelled * in Fig. 18) such that the spectra of *R*,*R*-[VO(**1**)] in *S*-epoxide and *S*,*S*-[VO(**1**)] in *R*-epoxide (Fig. 18a,b) were identical to each other, while the spectra of the opposite diastereomers *R*,*R*-[VO(**1**)] in *R*-epoxide and *S*,*S*-[VO(**1**)] in *S*-epoxide (Fig. 18c,d) were identical. These individual ENDOR spectra of the epoxide derived ^1H peaks (confirmed

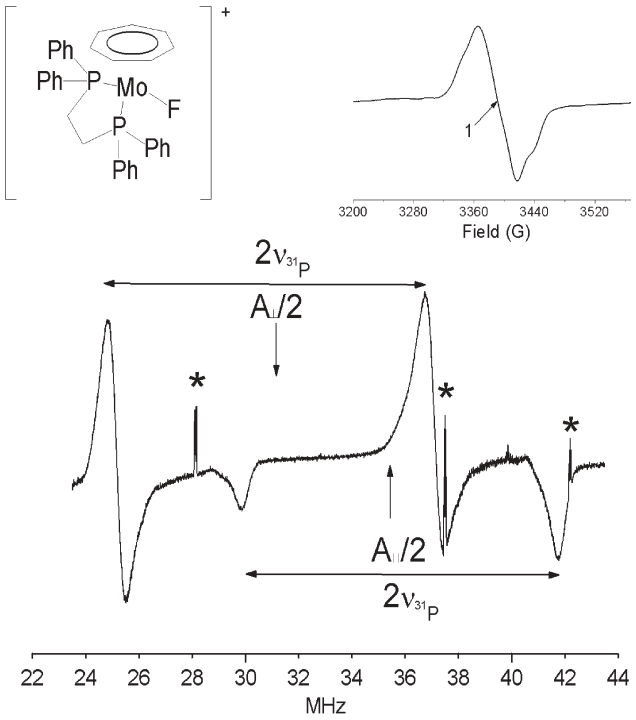

Fig. 16 cw-EPR and ^{31}P ENDOR spectrum of a $[MoF(dppe)(\eta\text{-}C_7H_7)]^+$ radical cation at 10 K. The field position for the ENDOR measurement is marked with an arrow in the EPR spectrum. The spikes marked * are due to instrumental artefacts.

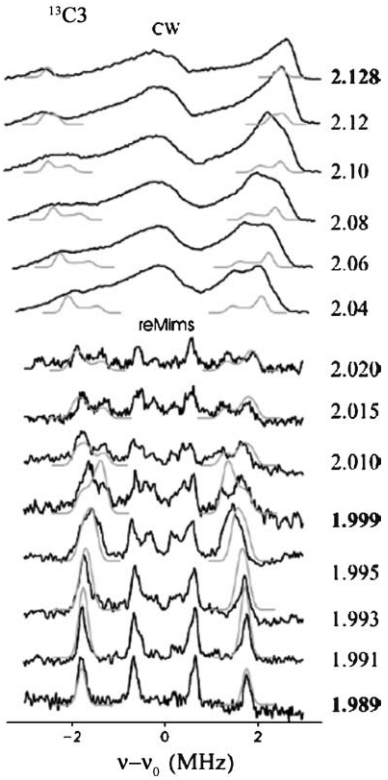

Fig. 17 Q-Band cw- and re-Mims pulse ^{13}C ENDOR spectra of an α-70^{Ala} variant MoFe protein (alanine substitution of the MoFe protein α-70^{Val} residue) turned over with ^{13}C labelled propargyl alcohol. The ENDOR spectra were measured as different field positions defined by the *g*-value shown on the right hand side. Reproduced with permission from ref. 27, © 2004 American Chemical Society.

with ^{2}H labelled epoxide) were simulated, to extract the dipolar contribution to the hyperfine tensor, and this provided an estimate of the $VO\cdots H_{epoxide}$ distance which was in excellent agreement with the DFT derived model. Furthermore by measuring the ENDOR spectra of the racemic [VO(**1**)] complex in racemic epoxide, it was possible to prove the higher stability of one diastereomer over the other (*i.e.*, Fig. 18e of the racemic experiment is identical Fig. 18c,d of the diastereomeric pairs *R*,*R*-[VO(**1**)] + *R*-epoxide and *S*,*S*-[VO(**1**)] + *S*-epoxide). This example illustrates how a three dimensional visualisation of diastereomeric interactions in solution, involving weak chiral interactions, can be generated by ENDOR measurements.

4.7 Asymmetric spin density distributions in copper porphyrin complexes

Metalloporphyrins have received considerably attention over the years due to their role in biology, medicine, material science and catalysis, and they have been widely studied by EPR and ENDOR in order to understand how the spin density is distributed around the ring. Recently, an unusual copper doped N-confused tetraphenylporphyrin complex (shown in Fig. 19) was prepared in order to elucidate the magntidue of the magnetic interactions between the unpaired electron of the copper and the nitrogen atoms of the porphyrin ring.[29] The EPR spectra of the complex magnetically diluted into a Zn(II) tetraphenylporphyrin powder were sufficiently well resolved that the inequivalencies in the three nitogens could be determined, with two nitrogens possessing a large coupling ($A_\parallel \approx 593 \pm 3$ MHz) and one nitrogen with a smaller coupling ($A_\parallel \approx 29.5 \pm 3$ MHz). However, the hyperfine and nuclear quadrupole couplings could be determined more precisely by pulse ENDOR spectroscopy. The Q-band Davies ENDOR spectra, measured at different magnetic field positions, are shown in Fig. 19. The ENDOR spectrum, recorded at a $g_\parallel$ position, produces a doublet centred at 30 MHz and separated by $2\nu_n$ of 7.2 MHz (*i.e.*, twice the nuclear Larmor frequency) with unresolved nuclear quadupole interactions. Since the ^{14}N peaks for strongly coupled nitrogens are centred on $A/2$, this indicates a hyperfine couplings of 60 MHz along this direction. At the different observer positions, the ENDOR spectra are now more complex, as more than one hyperfine and quadrupole orientation is selected. In this case simulation of the ENDOR spectra is required revealing the principal values of the hyperfine (***A***) and nuclear quadrupole (***P***) coupling tensors of $(A_1, A_2, A_3) = (71.5, 58.3, 59.5)$ MHz and $(P_1, P_2, P_3) = (-0.87, 1.00, -0.13)$ MHz. The smaller coupling to the third inner ring ^{14}N and outer inverted ^{14}N nucleus were analysed by hyperfine sublevel correlation (HYSCORE) spectroscopy, and this example illustrates the need to utilise ENDOR and HYSCORE to provide a complete picture of interactions with strongly and weakly coupled nitrogens in any macrocyle complex.

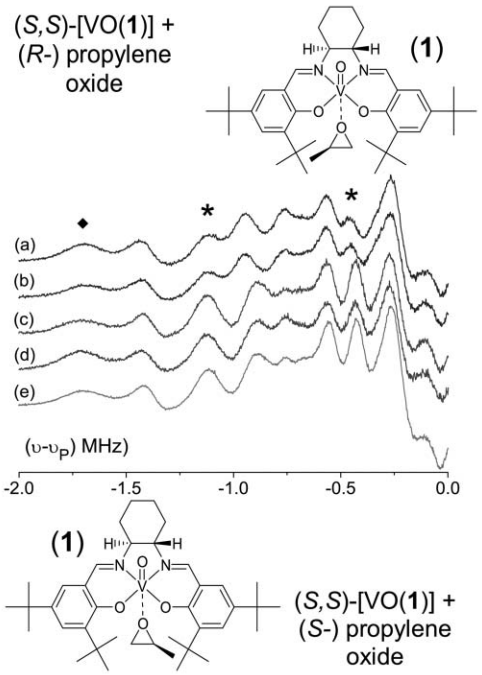

Fig. 18 X-Band ^{1}H ENDOR spectra (10 K) revealing the diastereomeric states formed between enantiomers of [VO(**1**)] dissolved in (*R*- or *S*)-propylene epoxide. (a) (*R*,*R*)-[VO(**1**)] in (*S*)-epoxide, (b) (*S*,*S*)-[VO(**1**)] in (*R*)-epoxide, (c) (*R*,*R*)-[VO(**1**)] in (*R*)-epoxide, (d) (*S*,*S*)-[VO(**1**)] in (*S*)-epoxide and (e) racemic (*RR*/*S*,*S*)-[VO(**1**)] in racemic (*R*/*S*)-epoxide. Reproduced with permission from ref. 28, © 2004 American Chemical Society.

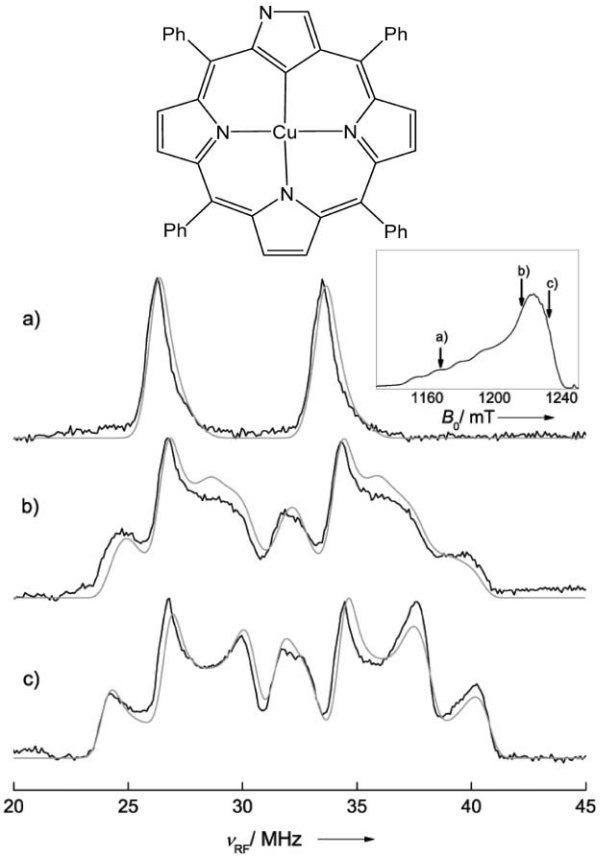

Fig. 19 Q-Band Davies ^{14}N ENDOR of a Cu(II) N-confused tetraphenylporphyrin complex diluted in a Zn(II) tetraphenylporphyrin powder. The FID detected Q-band EPR spectrum is shown in the inset, marking the different observer field positions. Reproduced from ref. 29 with permission from Wiley-VCH Verlag GmbH & Co.

4.8) Probing solvatochromic effects in an oxovanadium (IV) complex

Orientation selective ^{1}H ENDOR and complimentary DFT calculations were used to investigate the structure and conformational changes induced in an oxovanadium(IV) complex (vanadyl *N*,*N*′-bis(salicylidine)-1,2-ethylenediamine, abbreviated to VO-Salen) by changes in solvent system (*i.e.*, solvatochromism). The phenomenenon of solvatochromism is often defined as the (pronounced) change in position and sometimes intensity of an electronic absorption or emission band, accompanying a change in the polarity of the medium, and this definition can be extended to shifts in the resonance frequencies of an ENDOR transition from a ligand proton. By measuring the ^{1}H ENDOR spectra at the principle turning points in the EPR spectra of the VO-Salen complex in a protic and deuterated non-coordinating (dichloromethane, CH_2Cl_2) and coordinating (dimethylformamide, C_3H_7NO) solvents, subtle changes to the ligand conformations were detected in the "single-crystal" type ENDOR spectra by changes to the proton positions. The ligand coordinates of the geometry optimised structures (shown in Fig. 20 for the VO-Salen···DMF adduct), based on DFT caluclations, were compared to the proton coordinates determined by simulation of the ENDOR data (Fig. 20), based on the equations outlined in section 3. The geometrical distances between the unpaired electron and the ligand protons based on the two methods (DFT and ENDOR) were in excellent agreement. In the presence of a non-coordinating solvent (CH_2Cl_2), the expected square pyramidal symmetry of the V=O ion was confirmed both by ENDOR and DFT. However, in the coordinating solvent (C_3H_7NO), changes to the observed VO···H_{lig} distances in the ENDOR spectra evidenced the shift of the V=O group into the equatorial ligand plane through coordination with DMF. The axial coordination of the solvent, *trans* to the vanadyl oxo-ligand, was also confirmed by analysis of the hyperfine interaction to the DMF protons themselves. This example illustrates how very subtle changes to the ligand conformation of a transition metal complex, induced by solvent effects, can be examined in detail by ENDOR in frozen solution.

5 Concluding remarks

For any paramagnetic system, EPR and ENDOR spectrosocopies are clearly the methods of choice for a complete characterisation, since the two techniques combined provide unsurpassed detail on the electronic and geometric structure. Analysis of complex EPR spectra of organic radicals in solution is considerably simplified by ENDOR and TRIPLE resonance spectroscopy whilst in frozen solution and in the solid state, the spectra are more difficult to interpret, but the wealth of information that can be extracted from these powder

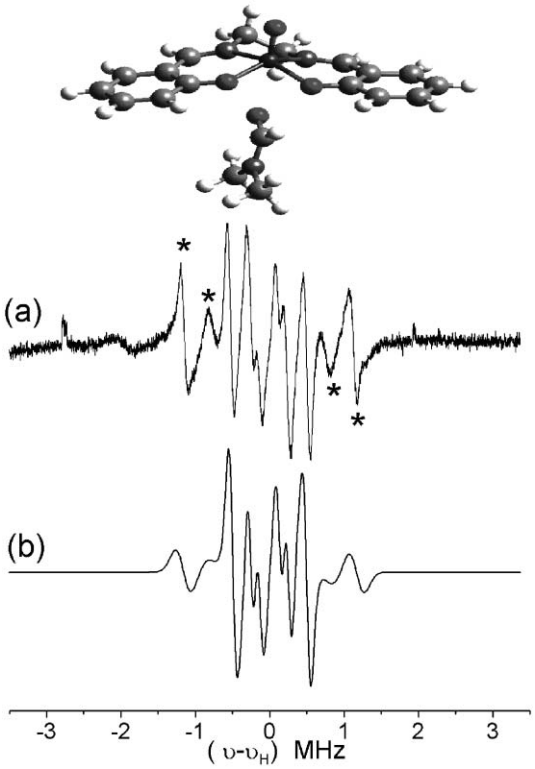

Fig. 20 X-Band ^{1}H ENDOR spectra (10 K) of a VO-salen complex (with deuterated ethylenediamine protons) dissolved in dimethylformamide. (a) Experimental, (b) simulated. The ENDOR spectrum was recorded at a static magnetic field of 2826G corresponding to the parallel hyperfine transition CCC (θ = 0°). The DFT minimised structure of the VO-salen···DMF adduct is also shown. The VO···H distances extracted from the simulated ENDOR data agreed with the structural model derived by DFT. Reproduced from ref. 30 with permission from Elsevier.

spectra is enormous. The local structure around the paramagnetic centre can be probed for example by analysis of the hyperfine and quadrupolar couplings, and the distances and angles between the paramagnetic centre and the interacting nuclei can be subsequently derived from the ENDOR spectra. This information can then be used as a starting point to model the local three dimensional structure of the paramagnetic species. While the analysis and interpretation of the orientation selective ENDOR spectra can be time consuming, and the extracted structural data from the hyperfine couplings may be based on approximations (*e.g.*, point dipole model) and assumptions, nevertheless the position of protons can be determined more precisely by EPR/ENDOR than by X-ray crystallography. Since ENDOR can give structural information in systems lacking long range order such as frozen solutions, polycrystalline powders, polymers or glasses, the need for single crystals is thus eliminated. Perhaps equally important are the ongoing applications and developments in quantum chemical calculations which are vitally important when the hyperfine couplings are required to provide detailed information on electronic and spatial structure. The role and importance of ENDOR spectroscopy for determining the structure and spatial distribution of a paramagnetic species in solution and in powdered systems has already been established, with many potential opportunities to apply the technique to more complex systems.

The range of sophisticated pulsed methodologies that are now available, and the continuing developments in instrumentation, certainly enhances the amount of information that can be spectroscopically retrieved. While this review has only considered cw-ENDOR methods, pulsed ENDOR methods (primarily based on the Mims and Davies sequences) are now routinely used.[18] In these experiments, the ENDOR signal is obtained by recording the echo intensity as a function of the RF pulse frequency. A change in the echo amplitude occurs when the RF is on-resonance with an NMR transition, thus generating an ENDOR signal.[15] In general ^{1}H spectra are best recorded by the Davies ENDOR sequence, whereas Mims ENDOR is preferred for ^{2}H measurements, so the pulsed method offers certain selective advantages for measuring ENDOR signals not feasible by the cw-methodology. ESEEM (or Electron Spin Echo Envelope Modulation) and its multidimensional extension HYSCORE, are also widely used methods. These are intrinsically time-domain techniques that employ the EPR spectrometer as an NMR detector and both ESEEM and pulsed ENDOR provide in effect complimentary information. According to Hoffman, on the applicability of both methods, "it need not be said that the best approach is to use a screwdriver on a screw, a hammer on a nail".[12] Whether the ENDOR data is collected by cw- or pulsed methods, it must still be interpreted and analysed to yield the structurally important information on the paramagnetic species, and orientation selective ENDOR is a key tool in this analysis.

Acknowledgements

We are grateful to the EPSRC for funding the former National ENDOR service at Cardiff University, and supporting many of the research areas covered in this article. The authors would also like to thanks G. Gescheidt, J. Rawson, G. Mitrikas and A. Schweiger for providing copies of their figures.

References

1 F. E. Mabbs, *Chem. Soc. Rev.*, 1993, 313.
2 L. Kevan and L. D. Kispert, *Electron Spin Double Resonance Spectroscopy*, John Wiley & Sons Inc, New York, 1976.
3 H. Kurreck, B. Kriste and W. Lubitz, *Electron Nuclear DOuble Resonance spectrosocpy of radicals in solution*, VCH Publishers, New York, 1988.
4 N. M. Atherton, *Principles of Electron Spin Resonance*, Ellis Horwood PTR Prentice Hall, Englewood Cliffs, NJ, 1993.
5 J. A. Weil, J. R. Bolton and J. E. Wertz, *Electron Paramagnetic Resonance; Elementary Theory and Practical Applications*, John Wiley & Sons, Inc, New York, 1994.
6 R. S. Eachus and M. T. Olm, *Science*, 1985, **230**, 268.
7 F. Gerson, *Acc. Chem. Res.*, 1994, **27**, 63.
8 A. Schweiger, *Struct. Bonding*, 1982, **51**, 1.
9 B. M. Hoffman, J. Martinsen and R. A. Venters, *J. Magn. Reson.*, 1984, **59**, 110.
10 (*a*) G. C. Hurst, T. A. Henderson and R. W. Kreilick, *J. Am. Chem. Soc.*, 1985, **107**, 7294; (*b*) T. A. Henderson, G. C. Hurst and R. W. Kreilick, *J. Am. Chem. Soc.*, 1985, **107**, 7299.
11 D. Attanasio, *J. Chem. Soc., Faraday Trans. 1*, 1989, **85**, 3927.
12 B. M. Hoffman, *Proc. Natl. Acad. Sci. U. S. A.*, 2003, **100**, 3575.
13 B. M. Hoffman, *Acc. Chem. Res.*, 2003, **36**, 522.

14 W. Lubitz, F. Lendzian and R. Bittl, *Acc. Chem. Res.*, 2002, **35**, 313.
15 D. Goldfarb and D. Arieli, *Annu. Rev. Biophys. Biomol. Struct.*, 2004, **33**, 441.
16 K. P. Dinse, *Advanced EPR – Applications in Biology and Biochemistry*, ed. A.J. Hoff, Elsevier, Amsterdam, 1989, chapter 17.
17 A. Schweiger, *Angew. Chem., Int. Ed. Engl.*, 1991, **30**, 265.
18 A. Schweiger and G. Jeschke, *Principles of Pulsed Electron Paramagnetic Resonance Spectroscopy*, Oxford University Press, Oxford, 2001.
19 G. Feher, *Phys. Rev.*, 1956, **103**, 834.
20 J. S. Hyde and A. H. Maki, *J. Chem. Phys.*, 1964, **40**, 3177.
21 G. H. Rist and J. S. Hyde, *J. Chem. Phys.*, 1970, **52**, 4633.
22 C. N. Simms, PhD Thesis, Cardiff University, 1998.
23 B. Grossmann, J. Heinze, T. Moll, C. Palivan, S. Ivan and G. Gescheidt, *J. Phys. Chem. B*, 2004, **108**, 4699.
24 A. Alberola, R. J. Less, C. M. Pask, J. M. Rawson, F. Palacio, P. Oliete, C. Paulsen, A. Yamaguchi, R. D. Farley and D. M.Murphy, *Angew. Chem., Int. Ed.*, 2003, **42**, 4782.
25 J. Luzon, J. Campo, F. Palacio, J. M. Rawson, R. J. Less, C. M. Pask, A. Alberola, G. McIntyre, R. D. Farley, D. M. Murphy, A. Goeta and J. A. K. Howard, *J. Am. Chem. Soc.*, 2005, submitted.
26 G. M. Aston, S. Badriya, R. D. Farley, R. W. Grime, S. J. Ledger, F. E. Mabbs, E. J. L. McInness, H. W. Morris, A. Ricalton, C. C. Rowlands, K. Wagner and M. W. Whiteley, *J. Chem. Soc., Dalton Trans.*, 1999, 4379.
27 H.-I. Lee, R. Y. Igarashi, M. Laryukhin, P. E. Doan, P. C. Dos Santos, D. R. Dean, L. C. Seefeldt and B. M. Hoffman, *J. Am. Chem. Soc.*, 2004, **126**, 9563.
28 I. A. Fallis, D. M. Murphy, D. J. Willock, R. D. Farley, R. Jenkins, R. R. Strevens and R. J. Tucker, *J. Am. Chem. Soc.*, 2004, **126**, 15660.
29 G. Mitrikas, C. Calle and A. Schweiger, *Angew. Chem., Int. Ed.*, 2005, **44**, 3301.
30 R. J. Tucker, I. A. Fallis, R. D. Farley, D. M. Murphy and D. J. Willock, *Chem. Phys. Lett.*, 2003, **380**, 758.

